

Design of a Variable Stiffness Vaulting Pole with Axial Spring

A mechanical model based exploration

Stein Posthuma

Master of Science Thesis
Faculty of Aerospace Engineering



Design of a Variable Stiffness Vaulting Pole with Axial Spring

A mechanical model based exploration

by

Stein Posthuma

in partial fulfillment of the requirements for the degree of

Master of Science

in Aerospace Engineering

at the Delft University of Technology,

to be defended publicly on December 13, 2018 at 11:00 AM.

Student number:	4024621	
Thesis committee:	Ir. J. Sinke,	Chairman
	Dr. ir. O.K. Bergsma,	Supervisor
	Prof. dr. F.C.T. van der Helm,	Reader
	Dr. ir. J.M.J.F. van Campen	Reader

An electronic version of this thesis is available at <http://repository.tudelft.nl/>.

Acknowledgements

I would like to express my gratitude to my supervisor Otto Bergsma for the useful comments, remarks and engagement through the learning process of this master thesis. Furthermore I would like to thank Marco Reijne for introducing me to the topic as well for the support on the way. Also many thanks to Frans van der Helm, for providing great feedback during the meetings at the biomechanical engineering department. Finally, I wish to thank my parents, my brother and sister, and Suus for their support.

*Stein Posthuma
Delft, December 2018*

List of Figures

2.1 Pole vault phases Frère <i>et al.</i> (2010)	5
2.2 Energy transformation showing the flight path of a vaulter (Burgess, 1998)	6
2.3 Typical curves of kinetic energy (black line), potential energy (grey line), and mechanical energy (dashed lined) of the athlete and total strain energy of the pole (dotted line) during the pole vault (Frère <i>et al.</i> , 2010)	6
2.4 Pole-vaulter forces and moments, exerted on the pole (Morlier and Mesnard, 2007)	7
2.5 Ground reaction force during vault	8
2.6 Pole in horizontal position with the weight and forces from the top- and bottom hand acting on it	8
2.7 Material property charts to determine the material index (Ashby and Cebon, 1993)	10
2.8 Two cross-sections of the pole Burgess (1998)	11
2.9 The thin solid line shows the trajectory of the vaulter. The vaulter and pole are shown at the instant of take-off, maximum pole bend, pole release and the peak of the vault. (Linthorne, 2000)	12
2.10 Pogo stick with a mechanical (coil) spring	14
2.11 Air spring (IGS, 2017)	14
2.12 Simplified design of pole and spring system	15
2.13 Initial and compressed spring, in which the sealant is clearly shown	16
2.14 Normal force profile	16
2.15 Response of the spring	17
3.1 Schematic diagram of the pole vault (Reijne, 2016)	20
3.2 Schematic diagram of a fictitious pole subjected to an end force only (Reijne, 2016)	21
3.3 Definition of the amplitude angle ϕ (Reijne, 2016)	22
3.4 Simulation of a vault using a constant stiffness pole	23
4.1 Deformation of a constant stiffness pole subjected to an end force and end moment. The input parameters are given in Table 4.1	26
4.2 Deformation of a variable stiffness pole subjected to an end force and end moment. The input parameters are given in Table 4.2	27

4.3	Variable stiffness pole vault	29
4.4	Deformation of a 1-segment pole and a 4-segment pole. Pole properties are given in Table 4.5. The compressive end force R is found to be $-1019 N$	30
4.5	The compressive force R during 2 simulated vaults. A 1-segment pole is used for one vault and a 2-segment pole, consisting of the same properties, is used for the other vault.	31
4.6	Vault with an axial spring	32
4.7	Spring response	32
5.1	Control torques obtained by trial and error (Reijne, 2016)	34
5.2	Optimized control torques	35
5.3	Vault at $t = 0.22 \text{ sec}$ for three different poles	36
5.4	Undesired spring response	37
5.5	Desired spring response	37
5.6	Desired spring response	38
6.1	Apply an end torque during pole bending and an opposite end torque during pole straightening (Fukushima <i>et al.</i> , 2013)	40
6.2	Elastica solution for a variable stiffness pole. The input properties are given in Table 6.1. The applied end torque is positive.	42
B.1	Schematic diagram of a fictitious pole subjected to an end force only (Reijne, 2016)	49
D.1	Elastica solution for a pole having a high stiffness in the middle (Pole 1). The input properties are given in Table D.1. The compressive end force R is found to be $-1429 N$	59
D.2	Elastica solution for a pole having a high stiffness at its ends (Pole 2). The input properties are given in Table D.1. The compressive end force R is found to be $-1095 N$	59
D.3	Elastica solution for a variable stiffness pole. The pole properties are given in Table D.2. The applied end torque T is $-1000 N \cdot m$. The compressive end force R is found to be $-832 N$	60
D.4	Elastica solution for a variable stiffness pole. The pole properties are given in Table D.2. The applied end torque T is $1000 N \cdot m$. The compressive end force R is found to be $-1861 N$	60
D.5	Elastica solution for a variable stiffness pole consisting of 16 segments. The pole properties are given in Table D.3. The compressive end force R is found to be $-1242 N$	61
D.6	Elastica solution for a variable stiffness pole consisting of 16 segments, including the fictitious poles. The pole properties are given in Table D.3. The compressive end force R is found to be $-1242 N$	61
E.1	Compressive force R and pole chord l during a vault. The MPB is indicated in the figure.	64

F.1 A variable stiffness 2 segment pole	65
G.1 Cross-sectional overview of the production process, using a female mould	69

List of Tables

2.1	Properties of the air spring	17
4.1	Input parameters for a constant stiffness pole	26
4.2	Input parameters for a variable stiffness pole	27
4.3	System properties, containing athlete- and pole properties	28
4.4	Initial conditions	28
4.5	Pole properties of two poles. Deformation is shown in Fig. 4.4	30
5.1	Pole properties of three poles, for which the control torques are optimized	35
5.2	Input parameters for a variable stiffness pole	36
6.1	Input parameters for a variable stiffness pole, subjected to a positive end torque	41
6.2	Relation between end torque T and compressive force R for a pole with properties given in Table 6.1	41
6.3	Segment properties and differences	42
D.1	Input parameters for two variable stiffness poles	58
D.2	Segment properties	58
D.3	Segment properties for a 16 segment pole	58

Nomenclature

Abbreviations

CFRP	carbon fibre reinforced polymer
FBD	Free Body Diagram
GFRP	glass fibre reinforced polymer
HP	peak height
IAAF	International Association of Athletics Federations
MPB	maximum pole bend
PP	pole plant
PR	pole release
PS	pole straightening
TD	touchdown
TD1	last touchdown
TO1	last take-off

Subscripts

0	initial
<i>a</i>	allowable
<i>atm</i>	atmospheric
<i>c</i>	chamber
<i>cm</i>	center of mass
<i>min</i>	minimum
<i>n</i>	normal
<i>s</i>	specific
<i>t</i>	tangential
<i>v</i>	vaulter

Symbols

η	angle between the X axis (global) and the x axis (pole)
γ	angle between the tangent and the x axis at the global origin
γ	heat capacity ratio
ω_1	time derivative of ϕ

ω_2	time derivative of θ	
ϕ	amplitude angle	
ϕ	angle between the vertical and the segment representing the arms	
ρ	density	
σ	stress	
θ	angle between the segment representing the arms and the segment representing the rest of the athlete	
θ	angle between the tangent at any location on the pole and the x axis	
A	cross-sectional area	
B	Bending stiffness (EI)	
D	diameter	
E	Young's modulus	
E	elliptic integral of the second kind	
F	force	
f	force vector	
g	gravitational acceleration	9.81 m/s^2
g	vector containing the degrees of freedom, expressed in generalized coordinates	
h	convective acceleration	
h	height	
I	mass moment of inertia	
K	elliptic integral of the first kind	
k	'stiffness' of the vaulter's body	
k	modulus	
KE	kinetic energy	
L	length	
l	chord length	
l	vaulter's segment length	
M	mass matrix	
M	material index	
M	moment	
m	mass	
N	normal force	
n	number of segments	
P	pressure	
PE	potential energy	

q	vector containing the independent generalized coordinates
R	reaction force
s	arc length
T	control torque
T	transformation matrix
t	time
V	volume
v	velocity
x	spring displacement
x	vector containing the degrees of freedom

Contents

Acknowledgements	iii
List of Figures	v
List of Tables	ix
Nomenclature	xiii
1 Introduction	1
2 Literature Review	3
2.1 Introduction	3
2.2 Methodology	4
2.3 Background information	4
2.4 Limitations	11
2.5 Steps to be taken	13
2.6 Conclusions	18
3 Mechanical Model for a Constant Stiffness Pole Vault	19
3.1 Equations of motion	19
3.2 Calculating the pole end force	20
3.3 Simulating a pole vault	22
4 Mechanical Model for a Variable Stiffness Pole	25
4.1 Finding R and γ	25
4.2 The dynamic model	28
4.3 Verification	29
4.4 Axial spring	30
5 Optimization	33
5.1 Control torques	33
5.2 Axial spring	35

6 Discussion	39
6.1 Opposite applied torque	39
6.2 Segment length discrepancy	40
6.3 Other limitations and simplifications	40
7 Conclusions and Recommendations	43
A Derivation of the equations of motion	45
B Derivation of the arc length and curve shape	49
B.1 Arc length	49
B.2 Curve shape	51
C Fourth order Runge-Kutta	55
D Elastica solutions of poles having a variable stiffness	57
D.1 Different stiffness distribution	57
D.2 Influence of the applied torque	57
D.3 A pole consisting of a large amount of segments	58
E Finding and updating the initial guess	63
E.1 Setting the initial guess	63
E.2 Updating the initial guess	64
F The non-linear system of equations	65
G Improving the production process	69
G.1 Female mould	69
G.2 Soluble or meltable mandrel	70
Bibliography	71

1

Introduction

Is improvement of pole vaulting performance still possible, or has the theoretical peak level already been achieved?

Looking ahead to the 2020 Tokyo Olympics, in 2016 the NOC*NSF asked the TU Delft Sports Engineering Institute to identify the possibilities of improving pole vaulting performance. Marco Reijne developed a mechanical model in which a vault can be simulated.

Firstly a literature study was performed. Background information on pole vaulting, such as energy transformation, loads and the design of the pole has been reviewed. The limitations have been assessed. These limitations can be used during the thesis. The literature study is presented in [Chapter 2](#).

During this research, as a follow up on the research of Reijne, several improvements have been made to the model. A method has been developed to include vaulting poles with a variable stiffness. It is investigated whether a variable stiffness vaulting pole influences pole vaulting performance, or whether it affects the flight path of the vaulter. It also has an effect on the weight distribution of the pole. The variable stiffness method is presented in [Chapter 4](#).

Furthermore, an axial spring was added to the pole at different locations. At pole-planting box impact, a significant amount of energy is dissipated. An axial spring reduces the amount of energy loss. The feasibility of this innovation has been reviewed and is shown in [Section 4.4](#).

Among other factors, the technique of the vaulter determines if a vault is successful. The control strategy of the athlete has been optimized for various vaulting poles. This is presented in [Chapter 5](#).

Finally, limitations and simplifications to the mechanical model are reviewed in [Chapter 6](#). The main conclusions and recommendations are given in [Chapter 7](#).

2

Literature Review

This literature review shows the limitations in pole vault performance and the possible steps that can be taken to overcome these limitations. The design philosophy in pole vaulting has remained the same during the last decades. The technique of the vaulter and the materials and structure of the pole has not been changed. This gives reason to believe that changing the design philosophy could improve pole vault performance. The goal of this review is to identify the possibilities to improve pole design. The pole-planting box impact can be considered as an inelastic collision during which some of the energy of the pole-athlete system is dissipated. Storing this energy by implementing a spring system in the pole is the most promising way to improve vaulting heights in the future. In addition, adding a spring system will reduce the impact force on the athlete, which will decrease the chance of injuries.

2.1. Introduction

Pole vaulting is an extremely dynamic and complex sport that requires high levels of athleticism, precision, and skill. Interaction between athlete and sports equipment is important in many sports, this is especially the case for pole vaulting. The pole is subjected to very large deformations to store and return energy. A good understanding of the mechanics of the vaulting pole and the energy exchange with the vaulter is essential for peak performance and improving vaulting technique.

In 2016 [Reijne](#) produced a new analytical model for pole vaulting. Reijne suggested that the highest achievable height in pole vaulting is yet to be achieved. The goal of this literature review is to investigate the possibilities for improving pole vault performance. To improve pole vaulting performance, most emphasis has been on the technique of the vaulter in research so far. This review will look for opportunities in pole design, while also incorporating the bio-mechanical factors of the athlete.

The following research question is defined:

What would be the optimal material properties and optimal design for the pole vaulting pole in terms of obtainable height of the vaulter, especially in relationship with jumping technique and bio-mechanical factors of the athlete?

In order to answer this question the limitations of the current pole vaulting pole should be identified. To understand these limitations, information about the technique of the vaulter, loads that act on the pole and the production process of the pole will also need to be assessed. This knowledge will be useful to identify the opportunities to improve the pole design and in turn improve pole vaulting performance.

2.2. Methodology

This section outlines the search strategy and selection criteria adopted for this review, and provides descriptions of the types of studies reviewed.

The main source for this literature review are scientific papers obtained from online bibliographic databases. The following websites were used: Google Scholar, ScienceDirect, Web of Science, Scopus and the TU Delft Library.

"Pole vaulting" was used as a search term, combined with other terms to obtain relevant literature. Firstly, broad terms such as "energy", "performance", "production", "manufacturing" and "design" were used. Later the search was narrowed down by adding more specific terms, such as "energy loss", "energy dissipation", "stress analysis", "pole plant" and "take-off". Also literature concerning spring systems was obtained, with no relation to pole vaulting.

Aside from the scientific papers, information was also obtained from informal interviews with specialists on pole vaulting. Marco Reijne graduated in 2016 on the subject by creating an analytical model which simulates the pole vault motion. Next to his thesis he also provided information during several meetings. More knowledge was collected during a meeting with the former Dutch decathlon coach Vince de Lange and decathlon specialist Eelco Sintnicolaas. Eelco is the 2013 European Champion heptathlon and pole vaulting is his best event. Further, on June 15th 2017, the 35th International Conference on Biomechanics in Sports took place. Here the applied session on pole vaulting was visited in which the energy exchange concept was explained by Falk Schade and Ralf Müller. Finally, prof. dr. ir. J. L. Herder, professor on Interactive Mechanisms and Mechatronics, gave his insight on possible spring systems.

Not all information was available. Some information about the manufacturing and design of the pole was found. However, information about e.g. the specific layup of the fibers, the type of resin used or the curing pressure and curing temperature during production could not be found. This is because pole manufacturers don't want to share their knowledge.

2.3. Background information

Firstly, the basic technique of pole vaulting will be presented in [Section 2.3.1](#). It is important to find out which part influences the design of the pole the most. Secondly, the energy transformation during a vault will be discussed in [Section 2.3.2](#). Thirdly, the loads that act on the pole during a vault will be assessed in [Section 2.3.3](#). The structure of a vaulting pole will be examined in [Section 2.3.4](#). The manufacturing technique will be reviewed in [Section 2.3.5](#).

2.3.1. Pole vault basics

Pole jumping competitions were known to the ancient Greeks. The sport is Olympic since 1896 for men and since 2000 for women. At first the poles were made of heavy, rigid hardwood. Due to technological innovations and improvement of the athlete's technique a switch was made to bamboo and later to aluminum poles. Today flexible composite poles are used to produce a slightly curved pole (pre-bend) that bends more easily under the loading caused by an athlete's take-off. The amount of fibers, fiber orientation and resin properties are carefully selected to provide the desired properties of the pole ([Linthorne, 2007](#)). Different fiber types are used to give poles specific characteristics to match each individual vaulter's style.

Pole vaulting is a dynamic sport that combines strength and technique to catapult, by using a pole, an athlete into the air over an elevated bar. Prior to jumping, a vaulter aligns the pole properly, so that the initial bend allows it to deform easier during the jump.

There are four phases of importance to be distinguished before the vaulter can pass the bar. The

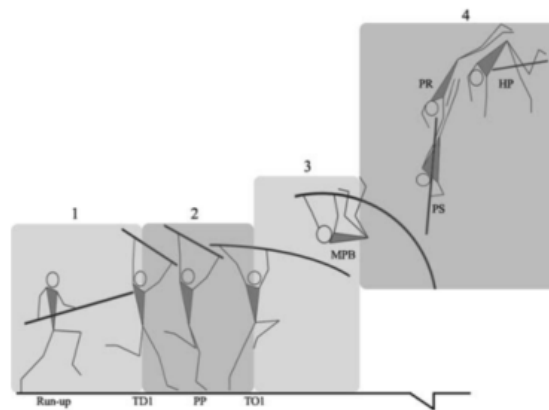


Figure 2.1: Pole vault phases Frère *et al.* (2010)

phases are shown in Fig. 2.1

1. The run-up phase which entails everything up to the last stance. The vaulter tries to increase his kinetic energy as much as possible, while carrying the pole.
2. The take-off phase is important and complex phase, during which the vaulter starts to jump and also plants the pole into the planting box. This all happens during the last stance in a very short period of time (approximately 0.16 s (Morlier and Mesnard, 2007))
3. The pole bending phase, in which kinetic energy is stored as spring energy into the pole.
4. The pole straightening phase, here the spring energy is given back to the athlete as kinetic and potential energy.

The design of the pole is most important during the second, third and fourth phase. During the second phase, the pole impacts planting box, during which energy is lost (inelastic collision). During the third and fourth phase, the pole design influences the time to maximum pole bend (MPB) and energy release (recoil speed), as well as the amount of energy stored in the pole. Hereafter the fifth phase, the fly-away phase, takes place. This phase does not influence the pole design.

2.3.2. Energy transformation

In mechanical terms the energy transformation entails generation of as much kinetic energy as possible by the athlete in the run-up phase and then use a long flexible pole to convert as much of this energy as possible into strain energy by bending this pole. When the pole straightens the strain energy will be converted into potential energy and kinetic energy (the athlete is accelerated upwards). Heavier athletes or athletes with a very high run-up velocity (Olympic vaulters) use a relatively stiffer pole since they have more kinetic energy.

The vaulter should follow a smooth path and should be able to rotate their body, therefore the bending stiffness of the pole should not be too high. The stiffness rating of a pole is 75 to 100 kg, which corresponds to an Euler buckling load of approximately 750 N to 1000 N. The path a vaulter follows with a flexible pole can be considered smooth in contrast to using a less flexible (or rigid) pole. This is shown in Fig. 2.2. The athlete would store less energy in a stiffer pole and transfer its kinetic energy directly into potential energy. However this sudden acceleration is not preferred as it would cause a significant energy loss at take-off (Burgess, 1998).

Further, with more bending, a higher strain energy is stored in the pole. Note that the amount of stored energy is limited by the material strength. A pole can be bend over 170° without breaking

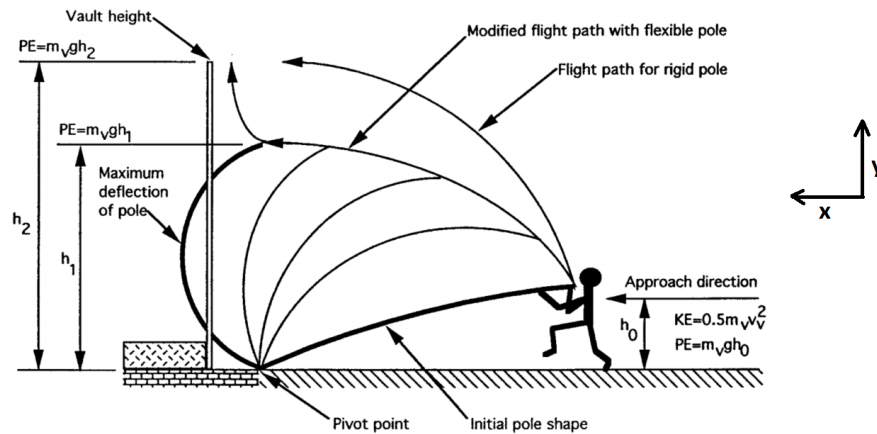


Figure 2.2: Energy transformation showing the flight path of a vaulter (Burgess, 1998)

(Linthorne, 2007). The amount of energy stored during this bend is approximately half of the vaulter's run-up kinetic energy (Linthorne, 2000; Nielson, 2006).

During the vault the vaulter applies a compressive force and a bending moment to the upper end of the pole while the bottom end is free to pivot in the planting box (Hubbard, 1980a; Griner, 1984). Arampatzis *et al.* (2004) distinguishes two parts of energy transformation. During part I there is transfer of energy of the athlete to the pole. Kinetic energy and muscular work of the athlete is converted into strain energy. The amount of muscular work is assumed to be 20% of the total mechanical energy of the athlete-pole system, according to Hubbard (1980a). This value is confirmed by Arampatzis *et al.* (2004). During part II of the athlete-pole interaction, the pole gives back energy to the athlete. Again muscular work is added by the athlete to the system. In Fig. 2.3 the amount of energy of the athlete and pole is given during a vault.

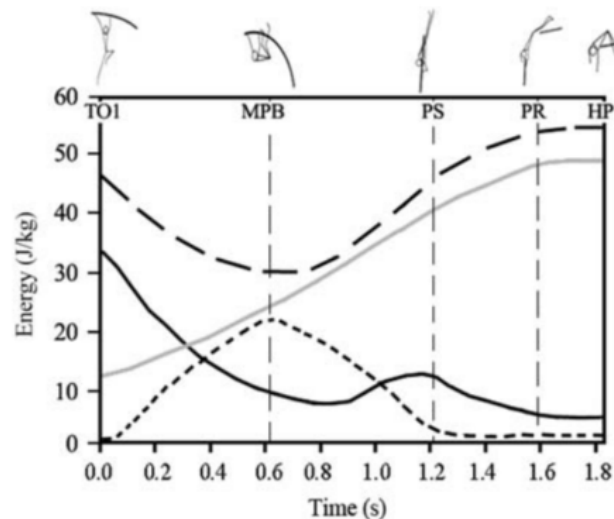


Figure 2.3: Typical curves of kinetic energy (black line), potential energy (grey line), and mechanical energy (dashed lined) of the athlete and total strain energy of the pole (Frère *et al.*, 2010)

2.3.3. Loads

The loading on the pole during vaults has been measured and is published in various papers. A distinction can be made between the ground reaction forces and the applied force and moment by the athlete. The applied force and moment has been measured by using two cameras to capture the 3D

movement of the vaulter (Morlier and Mesnard, 2007). The results are shown in Fig. 2.4.

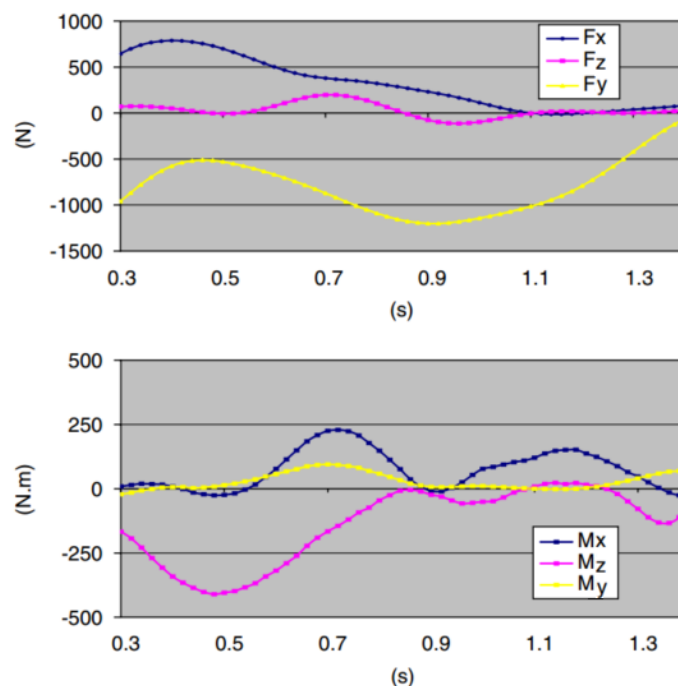


Figure 2.4: Pole-vaulter forces and moments, exerted on the pole (Morlier and Mesnard, 2007)

The axis system is a fixed system, as defined in Fig. 2.2. It can be observed that the force component along x remains positive during the jump, as the vaulter decelerates during the jump. Note that even though the pole is under compression, the force in x direction is positive, because of chosen the axis system. The force in the y -direction is related to the acceleration of the vaulter's centre of gravity. During the pole bending stage, the athlete rotates around his hips. This make is possible to apply a negative moment around z . Hereafter, the vaulter will also apply a moment around x and y , which will remain low compared to the z component. The applied bending moment around z is an important performance criterion. A large applied bending moment will result in a larger bend of the pole, adding more energy to the system.

The ground reaction forces have been obtained in multiple studies, by force plates or dynamometers. The relation is similar in all studies, apart from the force at impact. This can be seen in Fig. 2.5. The vertical component (F_y) increases until Maximum Pole Bend, and then decreases. The horizontal component decreases after impact, as the athlete keeps decelerating in this direction. The order of magnitude is equal for both reaction forces. The maximum force at impact varies between 500N and 2000N for the force in run-up direction and between 500 N and 2400 N for the force in upward direction. Reason for this variation might be that the measurement system cannot accurately measure such a high force, which is applied for a very short period of time. As the angle between the ground and the pole is approximately 30 degrees, the horizontal reaction force is most likely larger than the vertical reaction force at impact.

2.3.4. Material, structure and design

Poles are made of GFRP or CFRP. A small section of kevlar is added to the base of the pole to absorb the impact with the planting box (Burgess, 1998). For Olympic pole vaulters, the length of the pole is in the region of 5.4 m.

The pole is a thin walled tube and has an average weight of 1.5 to 3 kg. Reijne (2016) assumes that a lighter pole will not increase the run-up speed any further, as the speed is not limited by the

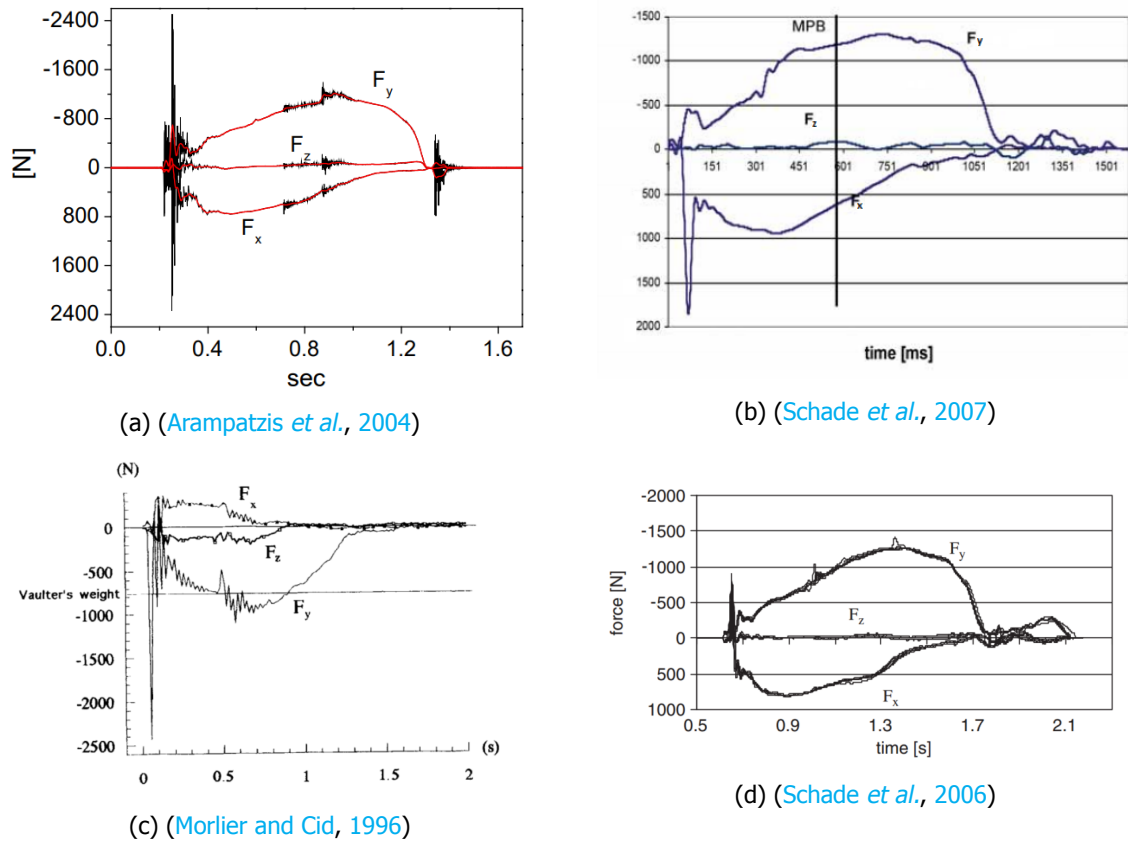


Figure 2.5: Ground reaction force during vault

weight of the pole but by the restriction of arm movement. The carry weight of the pole is next to the weight also an important factor. The carry weight can be calculated with Fig. 2.6. The pole is shown with the weight acting in the middle of the pole, assuming a uniform weight distribution. The top hand is the hand closest to the end of the pole. This has to perform a pulling force. The bottom hand has to push the pole up. In Fig. 2.6 the distance between the two hands is assumed to be 0.5 m. The total length of the pole is assumed to be 5 m. The pole is in a horizontal position (at the end of the run-up phase). Assuming the pole does not rotate, a simple calculation can be made to calculate the pushing force R_A , also known as carry weight. The sum of the moments around B should equate to zero.

$$\Sigma M_b = -R_A \cdot 0.5 + 2kg \cdot 2.5 = 0 \quad (2.1)$$

The carry weight R_A is 10 kg in this case, which is 5 times the actual weight of the pole. The ratio carry weight over weight is a function of the distance between the top- and bottom hand. This ratio can go up to 7 according to Nielson (2006). A reduction in weight might still be beneficial to the run-up speed.

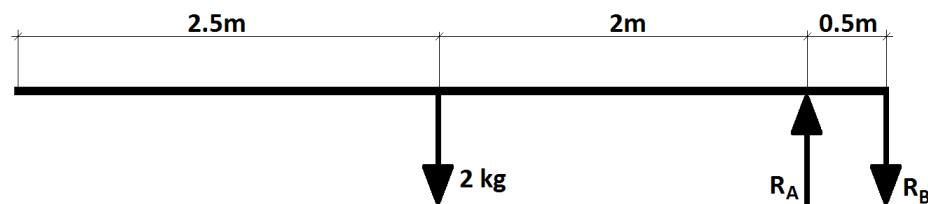


Figure 2.6: Pole in horizontal position with the weight and forces from the top- and bottom hand acting on it

According to Burgess, the pole has three main functions:

- Energy storage
- Act as pivoting column
- Provide the right stiffness

The energy storage function is important in the design process, because the pole is subjected to very large bending moments and stresses. The pole also has to provide bending stiffness in the x-z plane and torsional stiffness. The axis system is defined in Fig. 2.2. Torsional stiffness is required because of the initial bend of the pole. If the pole is not aligned properly the vaulter will experience a torque. The stresses due to bending in the x-z plane and torsion are small, relative to the stresses from bending in the x-y plane.

Burgess also defines the following design objectives for the pole:

- An energy storage capacity that matches the athlete's technique
- A stiffness distribution that matches the athlete's trajectory
- Minimize the mass of the pole in order to maximize the run-up velocity

To minimize the mass of an energy storage device, the stress distribution under maximal loading should be constant and equal to the maximum allowable (Boiten, 1963). This can be achieved by varying thickness. The optimal wall thickness distribution, for a constant stress, is a sine function, according to Boiten. The minimum wall thickness is approximately 1 mm in order to prevent local buckling. Varying the bending stiffness over the length of the pole could be another way of generating a constant stress distribution.

The radius of curvature should be constant for minimum mass, because in a thin walled tube the stress is proportional to the change in radius of curvature.

$$\sigma_a = \frac{ED}{2} \left(\frac{1}{R_{min}} - \frac{1}{R_0} \right) \quad (2.2)$$

In Eq. 2.2 σ_a is the maximum allowable bending stress, E is the Young's modulus, D is the mean diameter of the pole, R_0 is the initial radius of curvature and R_{min} is the minimum radius of curvature. The minimum radius of curvature at maximum deformation is an input requirement and defines the MPB. An initial radius of curvature is given to the pole to make initial bending easier. The center offset of the pole is approximately 50 mm. Davis and Kukureka (2012) states that the pre-bend of GFRP poles is about 20 to 30 mm. The ultimate vaulting pole should have a higher initial bend than the bend already applied to current poles (Burgess, 1998), since it is easier to bend a pole which is pre-bended. However this is difficult to produce. The material index that that should be maximized for minimum weight is derived by Burgess:

$$M = \left(\frac{\sigma_a^2}{\rho E} \right) \quad (2.3)$$

Here M is the material index, which is to be maximized by choosing the right material. σ_a is the maximum allowable stress, ρ is the density and E is the young's modulus.

This formula is also used by Linthorne (2007). The material index can be used to find the most appropriate material in Ashby and Cebon (1993). Eq. 2.3 can be rewritten to derive the following expression:

$$M = \left(\frac{\sigma_a^2}{\rho E} \right) = \left(\frac{\left(\frac{\sigma_a}{\rho} \right)^2}{E} \right) = \left(\frac{\sigma_s^2}{E_s} \right) \quad (2.4)$$

Here σ_s is the specific strength and E_s is the specific modulus. The right hand side of Fig. 2.7 is twice the resilience, which is the ability of a material to absorb energy when it is deformed elastically. Now Fig. 2.7 can be used to find the material which maximizes the index M . The materials to the right of the bold line are possible candidates. Polymers, foams and elastomers are too soft and are therefore excluded. The best practical material is CFRP, which is slightly better than GFRP or magnesium alloys.

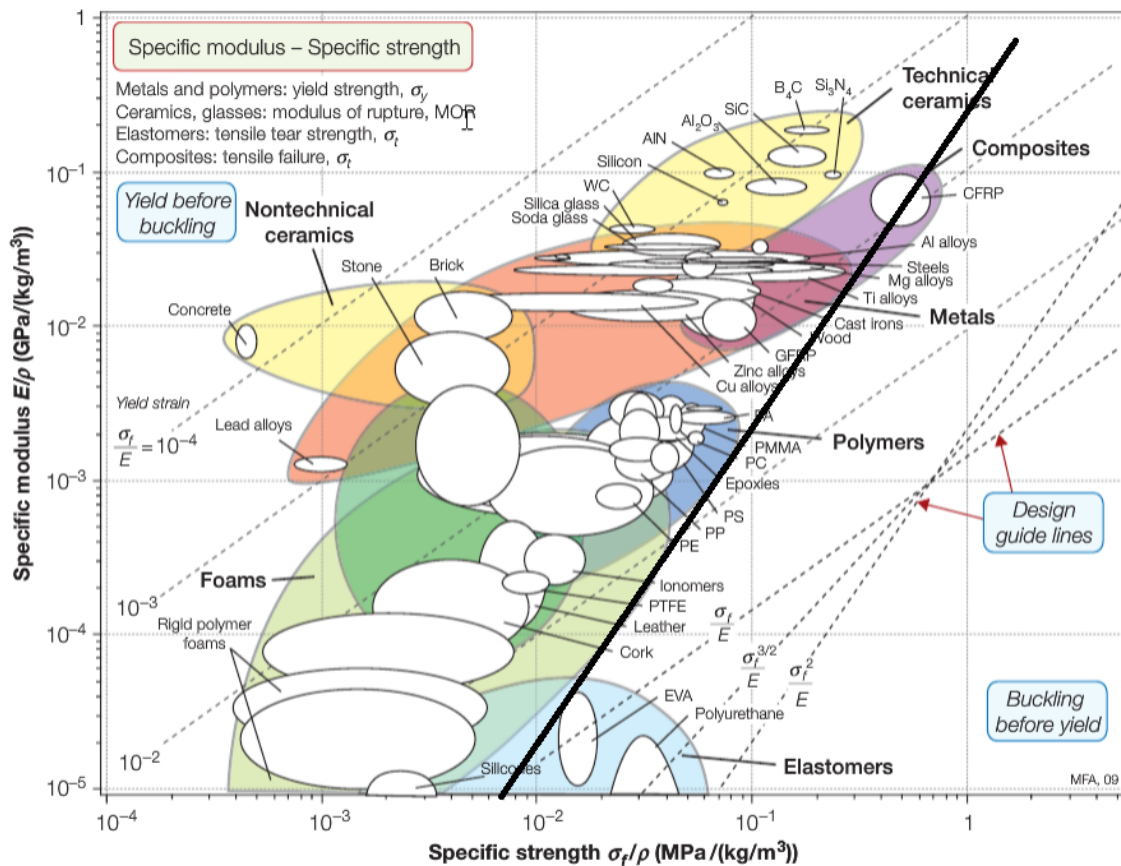


Figure 2.7: Material property charts to determine the material index (Ashby and Cebon, 1993)

The cross-section of the pole is circular. The diameter is typically about 40 mm, but depends on the vaulter. The outer diameter varies over the length for an optimum design. An elliptical cross-sectional area would be better in terms of energy storage capacity Burgess (1998). However, an elliptical shaped pole is more difficult to manufacture. Also an elliptical area provides less radial stiffness, causing the cross-section to flatten more easily.

The stiffness, weight and recoil speed of the pole are determined by the resin properties, the fiber properties, the orientation of fibers and the distribution of fibers along the length of the pole. The number and arrangement of fibers determines the mechanical properties, in particular the bending stiffness. The ability to tailor the material properties by using composites is a big advantage over isotropic materials. Several studies show that there is an optimal pole length and stiffness for each athlete, which maximizes the performance (Davis and Kukureka, 2012).

2.3.5. Production

Poles are manufactured for people of all skill levels and body sizes, with sizes as short as 3.05 to as long as 5.30 m, with a wide range of weight ratings. Each manufacturer determines the weight rating for the pole and the location of the maximum handhold band. It is unclear how manufacturers produce poles containing an initial bend. One method is to first produce a composite pole which acts as mandrel. This

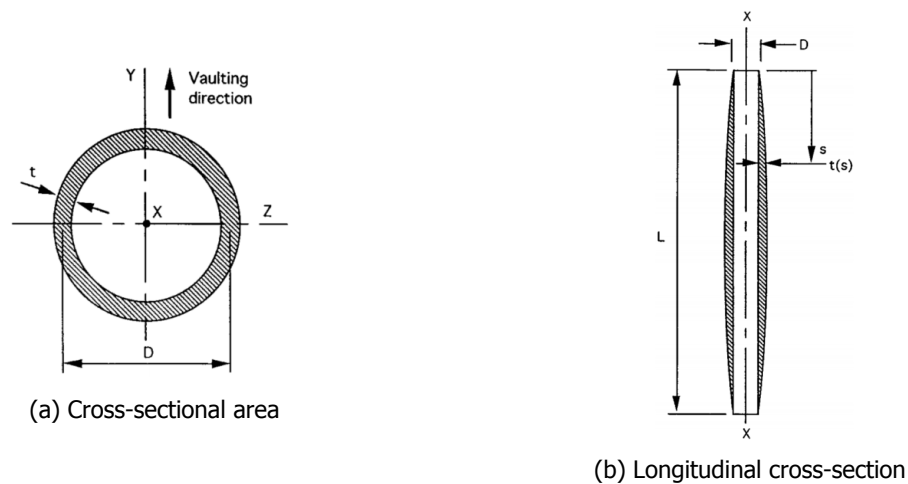


Figure 2.8: Two cross-sections of the pole Burgess (1998)

pole is held in a bent position while the main material is applied. The mandrel stays inside the final bend pole (Burgess, 1998). Another method is by orientating the mandrel horizontally and supporting it at its ends when curing the pole. The pole and mandrel bends because of its own weight. After curing the mandrel is removed (Strangwood and Subic, 2007).

According to Strangwood and Subic (2007), the pole is made up of three separate layers. All layers are fiber cloths pre-impregnated with epoxy resin (prepreg). The first layer is a narrow strip of cloth which is wound in a spiral around the mandrel (filament winding process). The machine that performs this action is called the (double) spiral wrapper. This first layer provides hoop strength and integrity to the pole. The fibers are oriented almost perpendicular to the length of the pole.

The second layer is called the body. It is a rectangular shaped piece of cloth wrapped fully around the mandrel, an X number of times, depending on the desired stiffness. The fibers are oriented mostly parallel to the length of the pole, hence this layer provides bending strength.

The third layer is known as the sail piece. This is considered the most important layer, as it determines the specific properties of the pole. It is a piece of cloth cut into a trapezoid shape (Davis and Kukureka, 2012; Strangwood and Subic, 2007). It determines the strength profile and bending stiffness distribution of the pole. The geometry of the sail piece determines where the pole has the smallest radius of curvature. This is often not constant over the length of the pole. Some athletes specify to the manufacturer the desired location as it suits their technique better.

2.4. Limitations

Pole vault performance is limited by energy losses during the vault and by limitations in pole design. These limitations will be assessed in Section 2.4.1 and Section 2.4.2.

2.4.1. Energy dissipation

Pole vaulting performance is determined by the kinetic energy at the end of the run-up and added muscular work of the vaulter. There are also substantial energy losses in the pole plant and take-off phases (Liu *et al.*, 2011; Linthorne, 1994). Johnson *et al.* (1975) calculated the energy loss at impact by modeling the vaulter as a point mass and as a uniformly distributed linear mass. He calculated the energy loss to be 50 % and 20 %, respectively. He concluded that the energy loss is likely to be much less than 20 %, for a professional vaulter, probably in the 10 % range. Research from Schade and Arampatzis (2012) showed that the energy loss is in the range of 2 % to 9 % of the initial energy.

During the applied pole vault session in Cologne Schade confirmed that the energy loss is approximately 10 % of the initial energy.

A distinction can be made between energy lost during the jumping action and energy lost when the pole is planted in the take-off box (Linthorne, 1994, Linthorne 2000, Schade et Al, 2012). During pole plant and take-off the vaulter's body acts as a damping system. Some of the kinetic energy is dissipated as heat in the vaulter's muscles, tendons and ligaments as the body is hyperextended. To jump up, the vaulter has to plant his foot in front of his center of gravity, to gain enough ground contact time to generate vertical velocity. This action also produces a horizontal braking force, thus decreasing its kinetic energy.

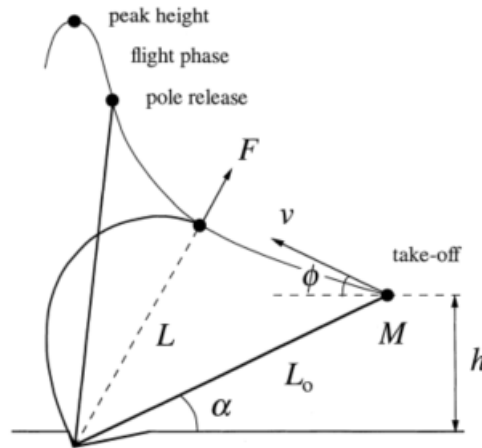


Figure 2.9: The thin solid line shows the trajectory of the vaulter. The vaulter and pole are shown at the instant of take-off, maximum pole bend, pole release and the peak of the vault. (Linthorne, 2000)

Linthorne considers the vaulter as a heavily damped linear spring which dissipates all energy. This makes sense as the damping coefficient of the human body is an order of magnitude higher than the pole and the planting box materials. The total energy dissipated in the vaulter's body can then be given by:

$$\Delta E = \frac{F_0^2}{2k} \cos^2(\phi + \alpha) \quad (2.5)$$

The total energy dissipated in the vaulter's body is given by ΔE . F_0 is the force exerted on by the pole on the vaulter, which is approximately the Euler buckling load, according to Linthorne. This force is squared, which means that the energy dissipated in the vaulter's body increases rapidly when stiffer poles are used. The constant k characterizes the 'stiffness' of the vaulter's body. Measurements of energy losses at take-off indicate that k is about 250 N/m for a world class vaulter (Gros and Kunkel, 1990; Angulo-Kinzler *et al.*, 1994). The angles ϕ and α are shown in Fig. 2.9.

2.4.2. Limitations of the pole design

The carry weight of the pole, which is up to 7 times the actual weight of the pole, could influence the run-up speed of the vaulter. The run-up velocity is the most important factor in pole vaulting (Linthorne, 2012) Therefore, the weight of the pole might still be a limiting factor and reducing the weight of the pole could improve pole vault performance. This assumption was also shared by Vince de Lange.

The initial bend is smaller than the optimum initial curvature. This is because the initial bend is limited by the current manufacturing method. A larger pre-bend could improve performance, as the pole can be deformed more easily.

The specific orientation of fibers and the distribution of fibers along the length of the pole is unknown, since pole manufacturers keep this a secret. It might be possible that the bending stiffness, strength or weight distribution over the length of the pole can still be improved.

2.5. Steps to be taken

The limitations in pole vault performance give rise to opportunities. These opportunities will be discussed in this section. Firstly, the possibilities in the model of Reijne will be discussed. Then the possibility of implementing an axial spring will be examined in [Section 2.5.2](#)

2.5.1. Analytical model of Reijne

[Reijne \(2016\)](#) developed an analytical model which simulates the vault from take-off until pole release. A big advantage of this model over a Finite Element model is that less computational time is needed. The model is unique, as the system consists of both the pole and vaulter. The motion of the athlete is described from take-off to pole release. The vaulter is modeled as 2-segment pendulum. Deformation, stresses and strains during the vault can also be obtained from simulation. The equations of motion are derived using a combination of the Newton-Euler method and Lagrange equations. The elastic problem is complex, as the slender pole is loaded by end forces and an applied moment and undergoes large deformations. This problem is solved by [Hubbard \(1980b\)](#), who applies a mathematical novelty, by introducing a fictitious longer rod with end forces only. The deformations can subsequently be solved.

[Reijne](#) used his mechanical model to simulate the motion of a vaulter using a pole with a spring. The results showed that the motion, forces and energy transformation are similar to that of a vault with a regular pole. However, the spring was modeled to be tangential to the chord of the pole, while it would be tangential to the lower part of the pole in reality (if implemented at that location).

2.5.1.1. Possible improvements of the model

The model of [Reijne](#) is most promising, compared to other analytical models, such as the model of [Walker and Kirmser \(1973\)](#) or the model of [Hubbard \(1980b\)](#). The model could be improved by adding variable stiffness over the length of the pole. Another step could be alignment of the spring with the tangent of the pole. The impact process is not taken into account in the simulation. Adding an impact sub-model could also be an improvement. Using a triple or quadruple segment pendulum instead of a double segment pendulum as athlete could also improve the model.

2.5.2. Adding a spring to the pole

As shown before, a significant amount of energy (about 10% of the total applied energy) is dissipated during the inelastic collision of the pole with the planting box. As the energy conversion during the rest of the vault is very efficient compared to the pole planting phase, reducing this energy loss by implementing a spring is the most promising way to improve performance. The spring would store energy at pole impact and give this energy back to the athlete. This will result in less energy dissipation, because the pole-planting box collision will be more elastic.

What would this spring look like? To answer this question it is important to look at the IAAF Competition Rules 2016-2017 on pole vaulting:

Athletes may use their own poles. No athlete shall use any other athlete's pole except with the consent of the owner.

The pole may be of any material or combination of materials and of any length or diameter, but the basic surface must be smooth. The pole may have layers of tape at the grip end (to protect the hand) and of tape and/or any other suitable material at the bottom end (to protect the pole). Any tape at the grip end must be uniform except for incidental overlapping and must not result in any sudden change in diameter, such as the creation of any "ring" on the pole.

Since the outer surface must be smooth and no sudden changes in diameter may occur, the only type of spring possible is a mechanical (coil) spring or air spring. In case of a mechanical spring, the coil should be covered with a smooth tube which would slide over the pole when compressed.



Figure 2.10: Pogo stick with a mechanical (coil) spring

The bending stiffness of the spring should be at least the same order of magnitude of the pole or higher, otherwise the curvature would prevent the outer tube to slide over the pole. The same principle has proven itself in the so-called Pogo stick. This device is shown in Fig. 2.10. It makes use of a coil compression spring or air spring. By the way it is designed, the spring system has enough bending stiffness so that it does not buckle.

2.5.2.1. Mechanical spring or air spring

A gas- or air spring consists of a precision rod attached to a piston moving within a sealed cylinder containing a gas, usually at an elevated pressure. The output force is the result of the differential between the pressure in the cylinder and atmospheric pressure outside the cylinder acting on the cross-section of the rod. As the piston rod is introduced into the cylinder, the internal pressure increases according to the volume of gas displaced by the rod.

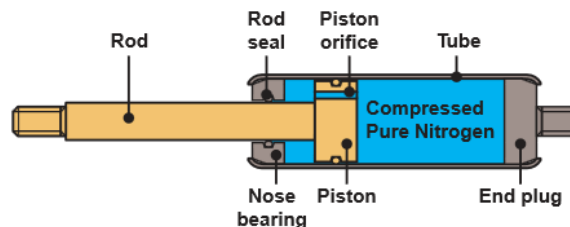


Figure 2.11: Air spring (IGS, 2017)

An air spring has several advantages over a coil spring. Because of the high pressure of the gas inside it, a gas spring can be much more compact than a metal spring that would provide the same amount of force. Gas springs expand and contract more smoothly than metal springs and can be designed to open and close at an exact and constant speed (unlike metal springs, which contract faster when they are extended further and can be very unpredictable). The mass of an air spring is less than a coil spring, which is the most important advantage. Because of these reasons, an air spring is preferred over a coil spring for this application.

The following parameters are important when designing the air spring:

- Weight (which is related to the carry weight)
- Friction

- Response

The weight is important with regard to the position of the spring. This will be discussed in the next section. The friction and response of the spring are also important. Two possible designs which respond to these characteristics are presented in [Section 2.5.2.3](#). The desired response of an air spring will be discussed in [Section 2.5.2.4](#)

2.5.2.2. Position of the spring

The athlete's muscles, tendons and ligament act as damping system when the pole impacts the planting box. The weight of the pole is negligible to the athlete's weight, therefore the position of spring is arbitrary; it could be implemented at either side of the pole.

A simplified design of the air spring is shown in [Fig. 2.12](#). Since the spring will be relatively heavier per unit length, compared to the rest of the pole, the best position for the spring might be at the end where the athlete holds on to the pole. This is because the carry weight will then be reduced. Looking at [Fig. 2.6](#), the location at which the weight of the pole acts will shift to the right. Using again a pole of 2 kg, if the center of gravity of the pole is at e.g. 2/5 of the pole instead of halfway, the carry weight will only be 8 kg. This is 4 times the actual weight of the pole, compared to 10 kg or 5 times the actual weight it was before.

Implementing the spring on the other end of the pole has the advantage that the extra weight does not have to be moved upwards. Therefore, the position of the spring is a trade-off and depends on the weight of the spring. If the added weight is small the spring would most likely be positioned on the end where the athlete holds on to the pole. Another possibility is to implement 2 springs at either side of the pole.



Figure 2.12: Simplified design of pole and spring system

2.5.2.3. Friction vs response: two possible designs

The outer cylinder will slide over the pole, which will generate friction and therefore loss of energy. This can be minimized by proper design and the use of a lubricant. If this spring has the same bending stiffness as the pole, it will also bend accordingly. When it bends the friction will increase. The spring could be designed having a greater bending stiffness, so that it barely bends. The rest of the pole could still bend to store energy and allow for a smooth flight path. In this way the energy losses due to friction will be minimized. A drawback of this design will be that the right response of the spring is difficult to control.

Preferably the spring is compressed until MPB. Hereafter it should expand again to return the energy to the athlete at the right time. This gives rise to a second design possibility. The bending stiffness of the spring and pole could be designed such that the spring is jammed when the pole is bend a certain amount. At this moment the spring is compressed. When the pole straightens again the spring 'unlocks' and return the stored energy to the athlete. The spring will respond as desired in this design. The downside of this design is that there will be more energy lost due to higher friction.

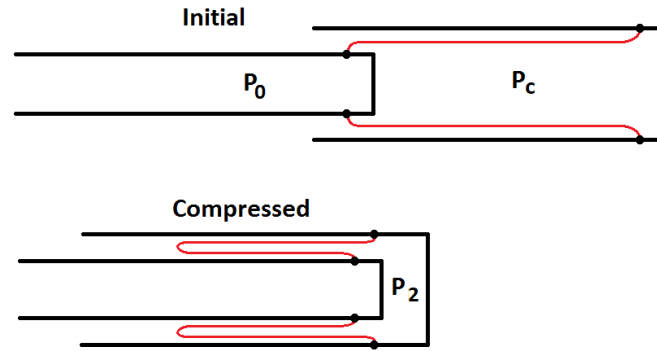


Figure 2.13: Initial and compressed spring, in which the sealant is clearly shown

2.5.2.4. Response of the air spring

In the initial condition air is compressed in the spring. This is shown in Fig. 2.13. The chamber is sealed hermetic by a polymer which rolls up when the spring is compressed. The amount of initial pressure determines the stiffness of the spring. Since the spring is compressed and expanded during a short period of time (approximately 1 second), the process can be considered adiabatic, which results in the following relation:

$$P \cdot V^\gamma = \text{constant} \quad (2.6)$$

In Eq. 2.6 P is the air pressure, V is the volume and γ is the heat capacity ratio, which is 1.4 for air. The initial force, which prevents the spring to be compressed, is given by Eq. 2.7.

$$F_i = (P_c - P_{atm}) \cdot A \quad (2.7)$$

Here P_c is the pressure in the chamber, P_{atm} is the atmospheric pressure and A is the cross-sectional area of the tube. Once the spring is compressed the pressure in the chamber will go up, which in turn will increase the spring force. The following differential equation can be derived for the motion of the air spring:

$$N(t) - A \left[\left(\frac{L_0}{L_0 - x(t)} \right)^\gamma P_0 - P_{atm} \right] = m \frac{d^2x}{dt^2} \quad (2.8)$$

Here N is the normal force acting on the spring, which is a function of time. L_0 is the initial length of

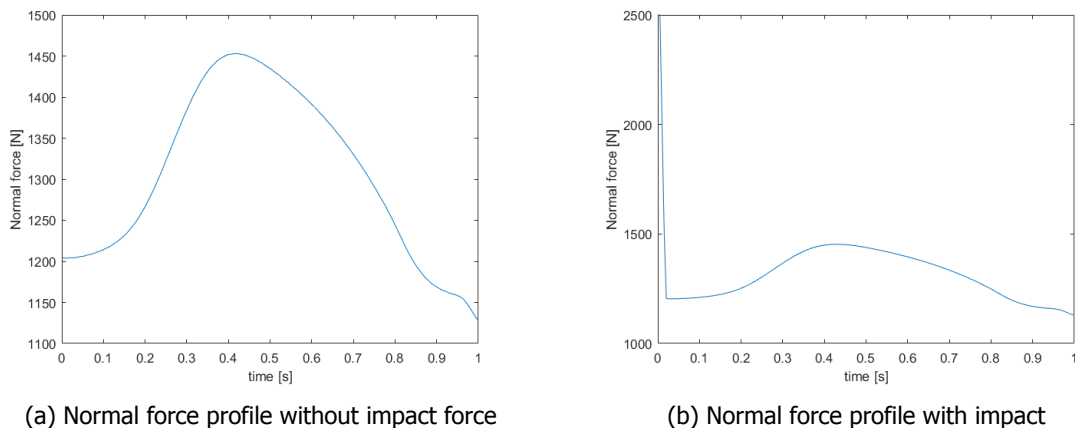


Figure 2.14: Normal force profile

the spring. P_0 is the initial pressure in the chamber. The displacement of the spring as a function of

time is given by $x(t)$. The displacement cannot be negative. The mass of the spring system is given by m . The normal force profile is obtained from the model of Reijne (2016). It is shown in Fig. 2.14a. The impact is not taken into account in the model. Using a vertical reaction force of 1500N and a horizontal reaction force of 2000N at impact, the normal force at impact can be calculated to be approximately 2500N. This impact force is added in the beginning of the profile and shown in Fig. 2.14b. The impact force is shown as a peak in Fig. 2.14b and it is assumed that this peak force is quickly damped.

Knowing the normal force profile as function of time, the differential equation can be solved numerically to give the time response of the spring. The response depends on the properties of the spring. The properties used can be found in Table 2.1. Note that the mass given in Table 2.1 is the mass of the

Table 2.1: Properties of the air spring

Initial length, L_i	0.9 m
Diameter, D	3 cm
Specific heat ratio, γ	1.4
Mass, m	80 kg
Atmospheric pressure, P_0	101325 Pa
Initial pressure, P_i	950151 Pa
Preforce, F_i	600 N

total system, consisting of athlete, pole and spring. The response of the spring is shown in Fig. 2.15.

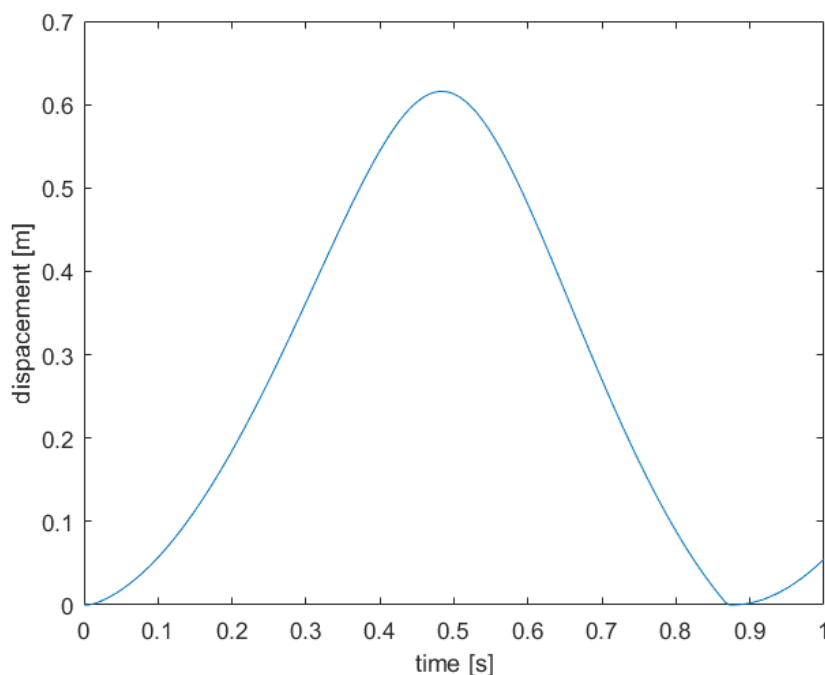


Figure 2.15: Response of the spring

The response of the spring is as hoped-for. It is desired that the spring is compressed and straightened during one complete vault. After 0.9 seconds the spring has returned all stored energy to the athlete. By changing the spring's preforce each spring system could be tailored to each specific athlete.

It is not necessary to jam the spring when it is fully compressed. This allows for a much simpler

design. It is preferred that the spring has a higher bending stiffness to minimize losses due to friction. The response of such a spring system should be analyzed in more detail.

2.5.2.5. Injury prevention

Even though the rules allow a spring to be implemented in the pole, such a radical change will often be prohibited in sports. Similar revolutions in other sports are the aluminum baseball bat and the shark suit in swimming. Both items promote the results in their sport, but are not allowed, because records from the past will then be too rapidly improved. However, in pole vaulting athletes are not able to jump often. Eelco Sintricolaas can only jump 6 to 8 times a day, and not multiple days in a row. This is because of the big impact on the shoulders when pole collides with the planting box. A spring will lower the impact on the shoulders, which will prevent injuries. This is a good argument to allow such an innovative design.

2.6. Conclusions

The goal of the review was to identify the limitations of the current pole vaulting pole. The following limitations were identified:

- Energy is lost during the inelastic pole-planting box collision. Approximately 10% of the initial energy is dissipated in the vaulter's muscles, tendons and ligaments.
- The weight or weight distribution over the length of the pole is not optimal, since it most likely reduces the maximum run-up velocity. By reducing the carry weight the vaulter can generate more kinetic energy.
- A larger pre-bend is preferred. The athlete will then be able to deform the pole more easily.

The second goal of the review was to identify the opportunities to improve the pole design and in turn improve pole vaulting performance.

- The analytical model of Reijne could be improved by adding variable stiffness over the length of the pole. Another step could be alignment of the spring with the tangent of the pole. The impact process is not taken into account in the simulation. Adding an impact sub-model could also be an improvement. Using a triple or quadruple segment pendulum instead of a double segment pendulum as athlete could also improve the model. A pole design can be created from the improved model, which might improve pole vault performance.
- Implementing an air spring in the pole is the most promising way of reducing the amount of energy losses at impact. This will result in higher vaults. Another advantage is that the impact on the athlete's shoulders is reduced, therefore athletes will be less injured. Preferably, the spring should compress during pole bending and expand during pole straightening. A simple model showed that this response is feasible.

3

Mechanical Model for a Constant Stiffness Pole Vault

A mechanical model had been developed by Reijne (2016) that simulates the motion of the athlete and the pole. This model is based on the work of Hubbard (1980b). In this analytical model, the motion starts just after the moment the athlete plants the pole in the planting box and ends at the time the athlete releases the pole. The theoretical height can then be calculated using an energy method, knowing the kinetic energy of the athlete at that point.

The model has been further developed to investigate the possibilities of a variable stiffness pole, with or without an integrated longitudinal spring. This will be presented in the Chapter 4. In this chapter a short overview is given to explain the mechanical model with a constant stiffness pole.

3.1. Equations of motion

The motion of the athlete-pole system can be described by classical mechanics. The model is simplified by splitting the system into one element for the pole, a rigid body for the arms of the athlete and a rigid body for the head, torso and legs of the athlete. The model is 2 dimensional. A FBD with the appropriate angles and lengths is shown in Fig. 3.1. The compressive force on the pole end exerted by the athlete is decomposed into a tangential and normal component. This force changes during the vault and can be solved numerically, which will be shown in Section 3.2.

The athlete will perform muscular work during the vault, which is represented in the model by a control torque at the pole end, T_1 ¹. A second control torque can be applied by the shoulders. This torque is shown as T_2 .

The system of the pole and the two-segment athlete has the following degrees of freedom:

- The X -coordinate of the center of mass of the segment representing the arms, X_{cm1}
- The Y -coordinate of the center of mass of the segment representing the arms, Y_{cm1}
- The angle between the vertical and the segment representing the arms, ϕ
- The angle between the segment representing the arms and the segment representing the rest of the athlete, θ

¹The athlete can apply this moment by pushing the pole with one hand and pulling with the other hand.

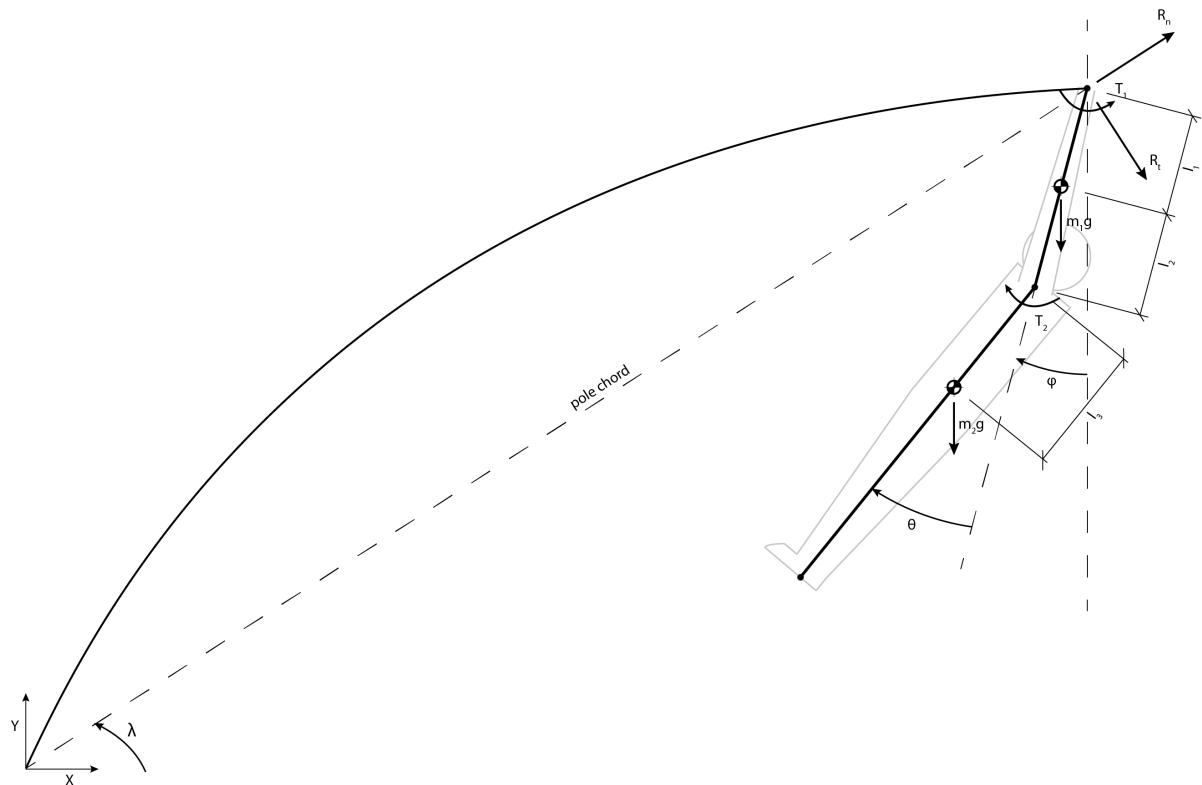


Figure 3.1: Schematic diagram of the pole vault (Reijne, 2016)

The location of the center of mass of the second segment and the location of the pole end, which is also the location of the top of the first segment, can be easily calculated from the above-mentioned independent generalized coordinates.

Several methods can be used to derive the equations of motion for multibody systems, like the Newton-Euler method or the Lagrange equations. A combinations of these methods is used, as this method is simple and computational efficient, as there is no symbolic computation of the partial derivatives needed. This combination of methods is known as the TMT method. (van der Linde and Schwab, 2011). The final form of the equations of motion is given by Eq. 3.1.

$$T_{i,k}M_{ij}T_{j,l}\ddot{q}_l = y_l T_{i,k} \sum (f_i + T_{i,k}M_{ij}g_j) \quad (3.1)$$

In Eq. 3.1 T is the transformation matrix, which relates the generalized coordinates to the positions and orientations of each body. The mass matrix is diagonal and contains the masses and inertiae of each body. The second derivative with respect to time of the generalized coordinates is given by \ddot{q}_l . The forces acting on each body are elements of the vector f_i . Finally, g_j is usually addressed as the convective acceleration. This term comes from taking the second derivative with respect to time of the degrees of freedom of each body. The derivation of the equations of motion for the athlete-pole system, resulting in Eq. 3.1, is given in Appendix A.

3.2. Calculating the pole end force

The pole end force R is required to solve the equations of motion. No elastica solution exists for a slender rod subjected to an end force and end torque. However, solutions exist for the case where the pole is subjected to a compressive end force only (Southwell *et al.*, 1941; Love, 1944).

Hubbard (1980b) uses this simpler case to derive the the elastica solution for a pole with a combined load of a force and moment at the end of the pole, like in Fig. 3.1. Imagine a fictitious constant stiffness rod loaded by an end force R only (the simpler, solvable case). This simpler case is shown in Fig. 3.2. The end force is aligned with the chord to enforce equilibrium. If the pole is cut anywhere a reaction force and a reaction moment can be found. This load case is similar to the combined load case. Now γ , which is the angle of the tangent to the pole at the global origin (Fig. 3.2) with the x axis, and R can be changed iteratively until the reaction moment at the cut is equal to the applied control torque, and until the chord length and pole length match the real pole chord length and real pole length.

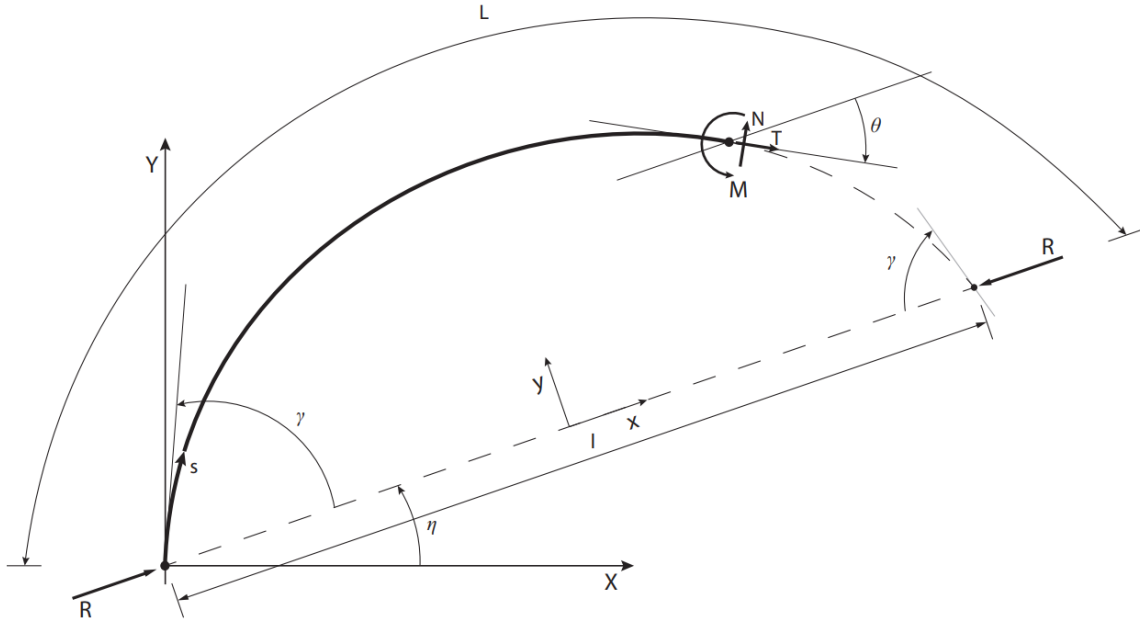


Figure 3.2: Schematic diagram of a fictitious pole subjected to an end force only (Reijne, 2016)

In order to solve numerically for γ and R , an equation for the arc length and curve shape of the fictitious rod needs to be derived. The arc length is given by:

$$s = \sqrt{\frac{B}{R}} K(k, \phi) \quad (3.2)$$

In Eq. 3.2 $K(k, \phi)$ is an elliptic integral of the first kind. The curve shape is given by:

$$x = \sqrt{\frac{B}{R}} (2E(k, \phi) - K(k, \phi)) \quad (3.3a)$$

$$y = -\sqrt{\frac{B}{R}} 2k \cos \phi \quad (3.3b)$$

In Eq. 3.3a $E(k, \phi)$ is an elliptic integral of the second kind.

The arguments k and ϕ can be derived from γ and θ , where θ is the angle between the tangent at any location on the pole and the x axis². The modulus k is defined as:

$$k = \sin \frac{1}{2} \gamma \quad (3.4)$$

²At the global origin γ is equal to θ .

The amplitude angle ϕ is defined as:

$$\sin \phi = \frac{\sin \frac{1}{2}\theta}{\sin \frac{1}{2}\gamma} \quad (3.5)$$

The variable ϕ is closely related to the distance along the arc of the pole. Its range is from $-\frac{\pi}{2}$ to $\frac{\pi}{2}$. The transformation is visualized in Fig. 3.3.

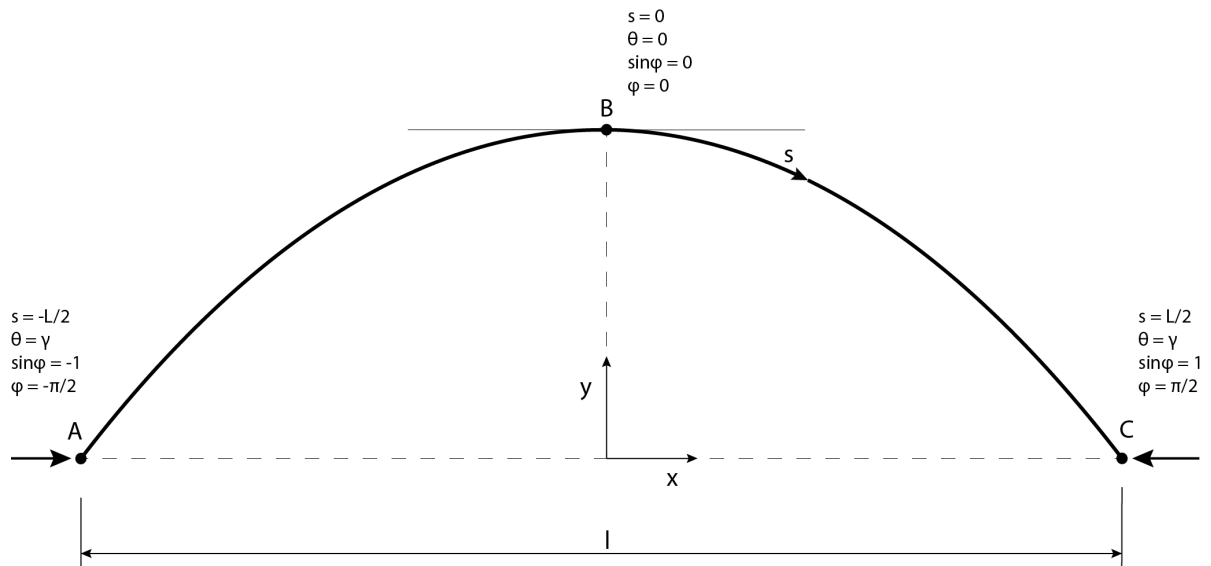


Figure 3.3: Definition of the amplitude angle ϕ (Reijne, 2016)

The curve shape coordinates x and y are calculated in the pole coordinate system. The location of the pole end can be calculated from the independent generalized coordinates (in the global coordinate system). The pole is rotated by an angle η until the pole end matches these coordinates.

The derivation of the arc length (Eq. 3.2) and curve shape (Eq. 3.3) has been done by Reijne (2016). A summary is shown in Appendix B.

3.3. Simulating a pole vault

Now that the pole end force has been calculated in Section 3.2, the equations of motion (Eq. 3.1) are integrated with respect to time, using a Runge-Kutta fourth order integration scheme. This integration scheme is used to solve first order differential equations. It is explained in Appendix C. The system of four second order differential equations is split into eight first order differential equations by taking the time derivatives of the independent generalized coordinates mentioned in Section 3.1.

$$\begin{bmatrix} v_x \\ v_y \\ \omega_1 \\ \omega_2 \end{bmatrix} = \begin{bmatrix} \dot{X} \\ \dot{Y} \\ \dot{\phi} \\ \dot{\theta} \end{bmatrix} \quad (3.6)$$

In order to solve the system of differential equations the initial conditions for the independent generalized coordinates (Section 3.1) and their time derivatives (Eq. 3.6) should be given as input.

At the end of the model when the athlete releases, the pole will be almost straight. At this point the total obtained height of the athlete can be simply calculated using a energy method ³.

³The kinetic energy in vertical direction at this point will be transferred to potential energy.

The mechanical model has been implemented in MATLAB. An example of a vault simulation is shown in Fig. 3.4. The vault takes approximately one second. Six instants are shown in the figure at $t = 0$, 0.2, 0.4, 0.6, 0.8 and 1 sec.

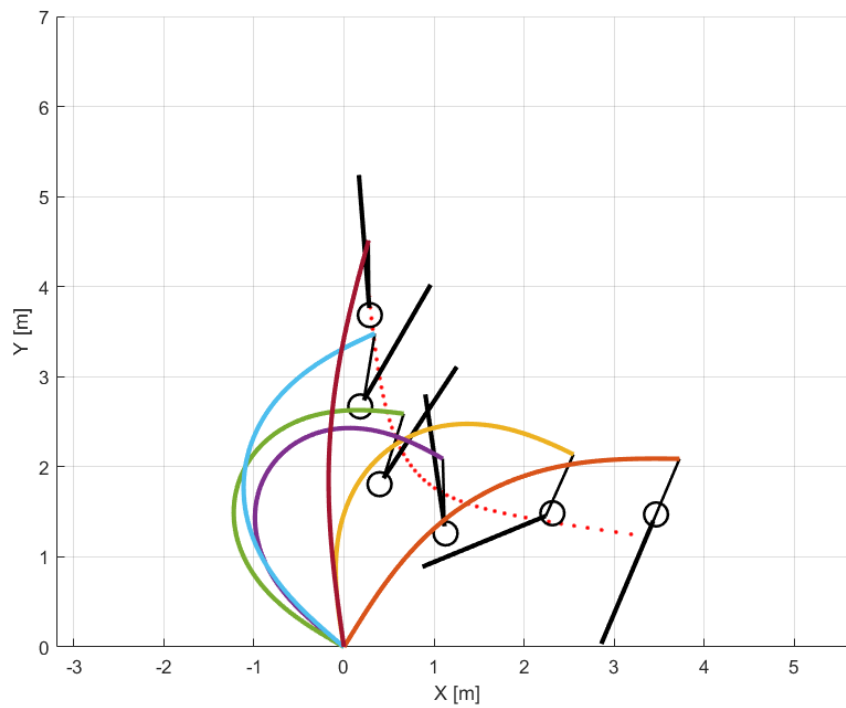


Figure 3.4: Simulation of a vault using a constant stiffness pole

4

Mechanical Model for a Variable Stiffness Pole

The mechanical model shown in [Chapter 3](#) only allows for poles with constant stiffness¹ along their length. A variable stiffness might improve the vault in various ways. The flight path could be influenced by the pole's stiffness. This could have an effect on the timing (control torques) of the athlete, or it could reduce the loss of energy during impact. The stiffness is also related to weight of the pole. More material added to a section of the pole will result in that section being heavier and stiffer. A variable stiffness could therefore also influence the carry weight ([Fig. 2.6](#)).

In order to add a variable stiffness pole to the model, first a method has to be found to calculate R and γ , just like for the constant stiffness pole. The location of the pole end is known. Also the stiffness and length of the different segments of the pole are assumed to be known, as well as the moment at the pole end, which is the control torque applied by the vaulter. The method to find R and γ is shown in [Section 4.1](#).

When R and γ are determined, the dynamic model can be updated for the variable stiffness pole. This is shown in [Section 4.2](#). This updated model is verified in [Section 4.3](#).

For the same reasons as for a variable stiffness pole, an axial spring added to the pole could also be an improvement. A spring has been added to the model. This is shown and its feasibility is discussed in [Section 4.4](#).

4.1. Finding R and γ

Just like in [Fig. 3.2](#), it is convenient to look at the pole in its own coordinate system. The pole can be easily rotated later by an angle η so that the the pole end is at the right location.

Using the method explained in [Section 3.2](#), the shape of a constant stiffness pole can be determined when the following parameters are known:

- The length L of the pole
- The chord length l
- The pole's stiffness B

¹Note that by stiffness here the bending stiffness EI is meant

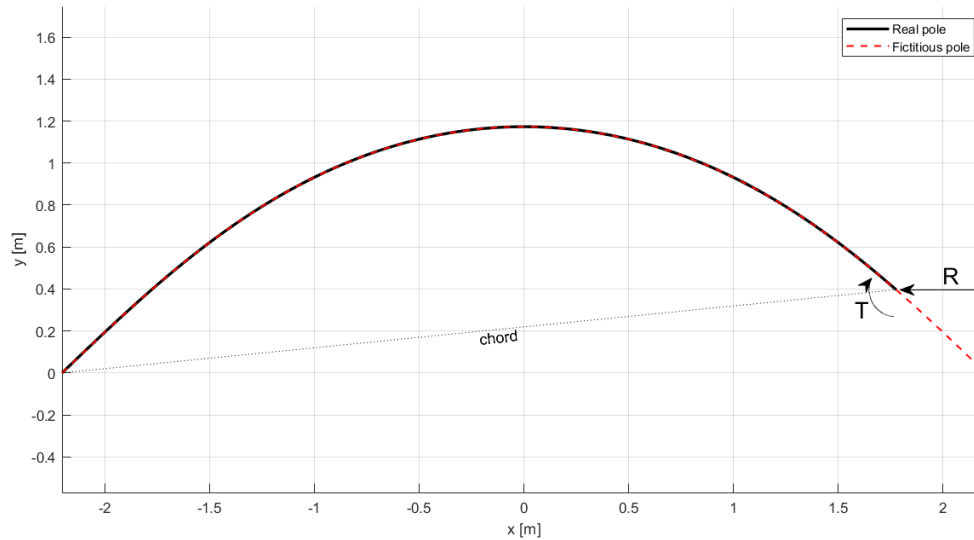


Figure 4.1: Deformation of a constant stiffness pole subjected to an end force and end moment. The input parameters are given in Table 4.1

- The moment T (control torque) at the pole end

The derived curve will be part of a fictitious curve, which represents the fictitious pole deformed by only an end force.

For example, given the parameters in Table 4.1, R and γ can be solved numerically. Subsequently, the curve shape can be determined with Eq. 3.3. After solving numerically, it is found that the angle

Table 4.1: Input parameters for a constant stiffness pole

Pole length, L	4.57 m
Chord length, l	4 m
Pole stiffness, B	2522 N · m ²
End moment, T	-800 N · m

of the pole with the x axis at the origin, γ , is -43.7° . The compressive force R is $-2017N$. The deformation of this pole is shown in Fig. 4.1. The fictitious pole is also plotted. The vertical distance between the x axis and the real pole end is $0.3967m$. A quick check shows that the determined force R corresponds to the applied torque: $R \cdot 0.3967 = -800Nm$.

Next a pole with a variable stiffness is inspected. To keep it simple, the pole is assumed to consist of only two segments. The input parameters are given in Table 4.2. They are similar to the constant stiffness pole of the previous example, in terms of total length, end moment and chord length.

The same conditions apply to the variable stiffness pole as for the constant stiffness pole:

- The fictitious pole should be cut at a certain location. At this cut the length should match the real pole length.
- At this cut the moment should be equal to the applied control torque.
- The length of a straight line from the beginning of the pole to this cut should be the length of the real pole chord

Table 4.2: Input parameters for a variable stiffness pole

Pole length, L	4.57 m
Length segment 1, L_1	$1/3L$
Length segment 2, L_2	$2/3L$
Chord length, l	4 m
Global stiffness, B_0	$2522 \text{ N} \cdot \text{m}^2$
Stiffness segment 1, B_1	$0.3B_0$
Stiffness segment 2, B_2	$2B_0$
End moment, T	$-800 \text{ N} \cdot \text{m}$

Apart from these conditions, the following boundary conditions are added for the variable stiffness pole:

- There should be a second cut where the two fictitious poles are connected. Each segment of the real pole is part of each fictitious pole. At this cut the lengths should match the lengths of each segment.
- At this cut the moment at the segment 1 should be equal to the moment at the segment 2.
- At this cut the tangent of each fictitious pole segment should be equal.

It turns out that there is only one force R , which can be applied to all fictitious poles. However, for each fictitious pole, there is a separate angle γ .

For the variable stiffness pole with input parameters as in Table 4.2, the end force R is found to be -746 N . The tangent at the origin for the first segment γ_1 is -73° , for the second segment γ_2 is -30° . The deformation of this pole is shown in Fig. 4.2.

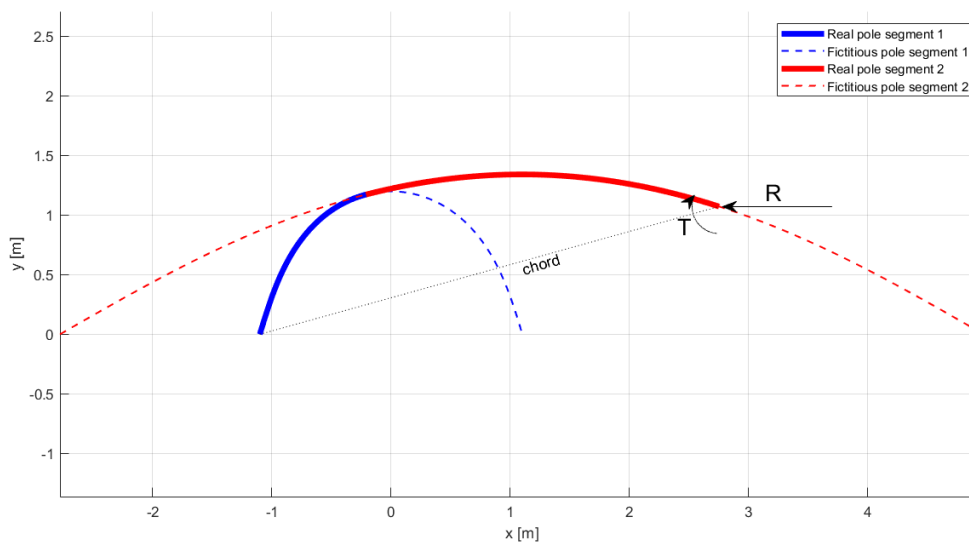


Figure 4.2: Deformation of a variable stiffness pole subjected to an end force and end moment. The input parameters are given in Table 4.2

It can be observed that the first segment, being much less stiff, is part of a smaller arc than the

second segment. The first segment is much more elastically deflected than the second segment, which is as expected. The vertical distance from the x axis to the pole end is $1.07m$. Multiplying this value with the found end force R gives indeed the applied torque of $-800Nm$.

Using the boundary conditions mentioned earlier, the elastica curves can be found for different types of poles. In [Appendix D](#) various deformed poles are showed, having different stiffnesses and consisting of different number of segments.

4.2. The dynamic model

A real vault as well as a simulated vault are greatly influenced by the following three factors:

- The initial conditions
- The system properties
- The control torques

The initial conditions are the generalized coordinates and their time derivatives at t_0 . The system properties consist of the athlete- and pole properties. The initial conditions and system properties of a top level vaulter have been derived from several studies ([Linthorne, 2000](#); [Adamczewski and Perlt, 1997](#); [Arampatzis et al., 2004](#); [Angulo-Kinzler et al., 1994](#); [McGinnis and Bergman, 1983](#); [Morlier et al., 2008](#); [Ekevad and Lundberg, 1995](#)). They are shown in [Table 4.3](#) and [Table 4.4](#). The same values have been used by [Reijne \(2016\)](#).

Table 4.3: System properties, containing athlete- and pole properties

m_1	20 kg	l_2	0.35 m
m_2	50 kg	l_3	0.4 m
I_1	2.96 kg · m ²	L	4.57 m
I_2	5.67 kg · m ²	B_0	2522 N · m ²
l_1	0.4 m		

Table 4.4: Initial conditions

X_{cm1}	3.57 m	ϕ	0.4 rad
Y_{cm1}	1.72 m	θ	0 rad
\dot{X}_{cm}	-8.7 m/s	$\dot{\phi}$	0.2 rad/s
\dot{Y}_{cm}	1.2 m/s	$\dot{\theta}$	0 rad/s

Using the system properties and initial conditions from [Table 4.3](#) and [Table 4.4](#), the pole will already be bend at the start of the simulation (at t_0). This is done for two reasons. Firstly, the pole-planting box impact is not taken into account. Secondly, the pole should be bend in the model in order to find a solution for R and γ . The straighter the pole, the harder it will be to find a solution.

During a simulation the general coordinates and their time derivative will be calculated iteratively, using the TMT-method described in [Section 3.1](#). During each iteration, values for R and γ_1 to γ_n will have to be determined numerically four times, since a fourth order Runge-Kutta integration scheme is used. The values are determined in MATLAB using the pre-programmed non-linear system solver

'fsolve'. This solver needs an initial guess for R and γ_1 to γ_n as input. The initial guess is critical in finding a solution. A method of finding a good initial guess and updating this initial guess when no solution can be found, is shown in [Appendix E](#).

The non-linear system of equations that needs to be established as input for 'fsolve' is also important when trying to find a solution. For an n -segment pole, $n + 1$ unknowns need to be determined, while there are $3n$ boundary conditions. An approach of dealing with this overdetermined system is described in [Appendix F](#).

The compressive force, the deformation of the pole and the flight path of the athlete depend on the initial conditions, system properties and the control torques during the vault. Therefore, when changing either of these three factors, one or both of the other factors should be changed as well to simulate a realistic vault.

A simulated vault, using a variable stiffness vaulting pole is shown in [Fig. 4.3](#). The arrows indicate the direction of the vaulter.

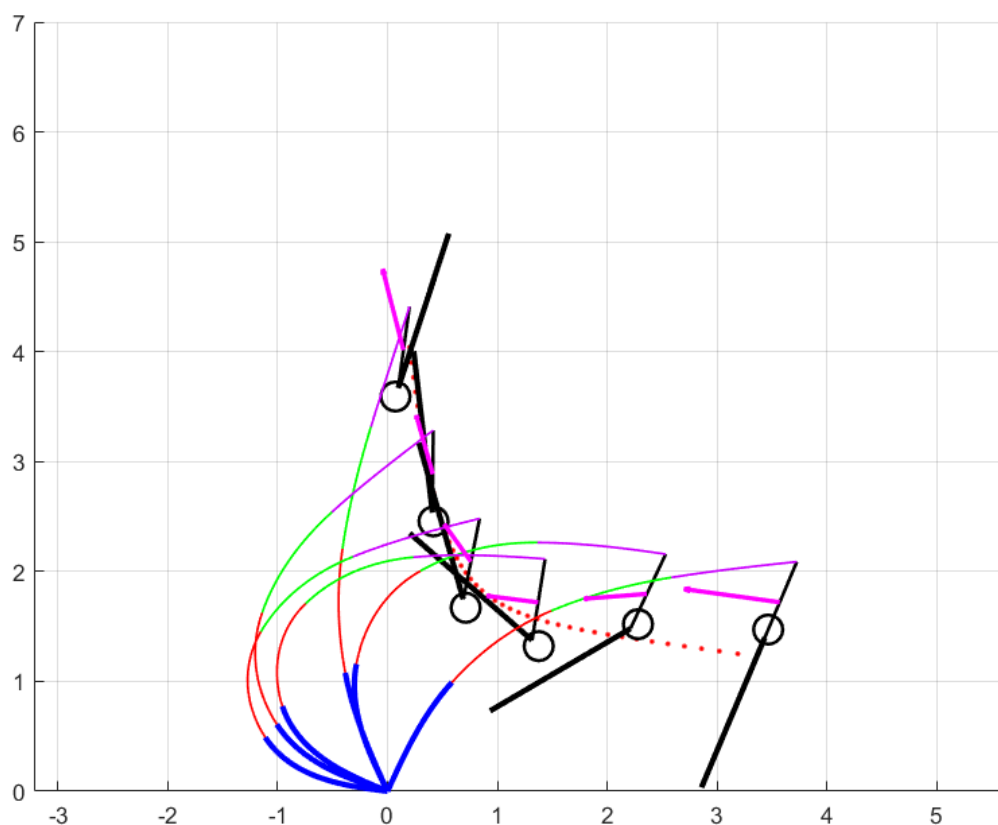


Figure 4.3: Variable stiffness pole vault

4.3. Verification

The variable stiffness model is verified by comparing it to the constant stiffness model. First the deformation of a 1-segment, constant stiffness pole is compared to a multi-segment pole. This pole consists of 4 segments, having different lengths. Each segment has the same stiffness as the 1-segment pole. The pole properties are given in [Table 4.5](#). The deformed poles are shown in [Fig. 4.4](#).

It can be seen that deformation of the two pole is exactly alike.

Table 4.5: Pole properties of two poles. Deformation is shown in Fig. 4.4

	1-segment pole	4-segment pole
Pole length, L	4.57 m	4.57 m
Length segments, L_i	$1L$	$1/10L, 3/10L, 2/10L, 4/10L$
Chord length, l	4 m	4 m
Global stiffness, B_0	$2522 N \cdot m^2$	$2522 N \cdot m^2$
Stiffness segments, B_i	$1B_0$	$1B_0, 1B_0, 1B_0, 1B_0$
End moment, T	$-400 N \cdot m$	$-400 N \cdot m$

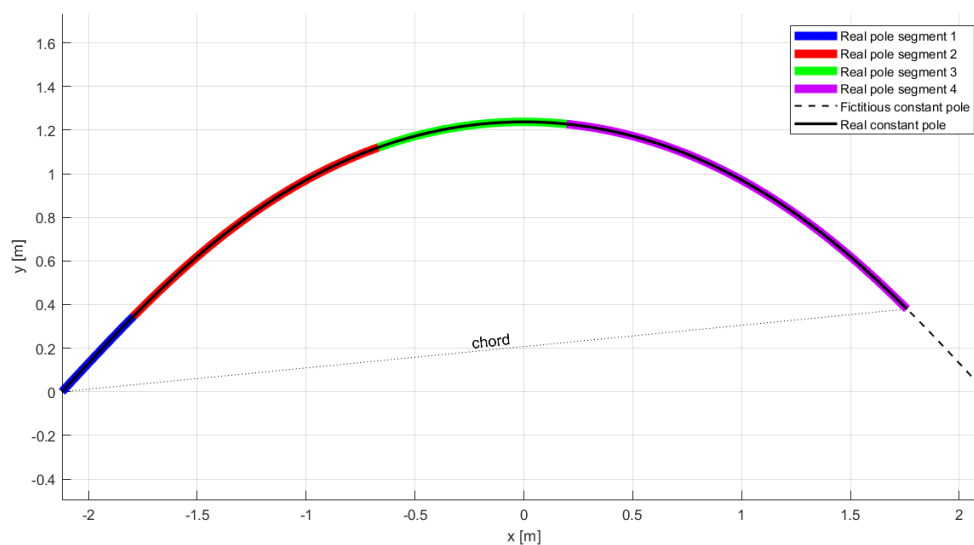


Figure 4.4: Deformation of a 1-segment pole and a 4-segment pole. Pole properties are given in Table 4.5. The compressive end force R is found to be $-1019 N$.

A second check is made by looking at a complete vault. One vault is simulated with a 1-segment pole, having the same properties as in Table 4.2. Another vault is simulated with a 2-segment pole, again consisting of the same stiffness and length as the 1-segment pole. The potential energy and kinetic energy in upward direction² at the end of the simulation is $4387 J$ for the 1-segment pole and $4332 J$ for the 2-segment pole. This results in a obtained height of approximately $6.39 m$ and $6.31 m$. The compressive force R during the vaults is shown in Fig. 4.5. The forces are almost equal. The small differences explain the difference in energy at the end of the simulations. The two vaults being almost identical validates the variable stiffness model as well.

4.4. Axial spring

An axial air spring could be added to the pole, to reduce the amount of energy dissipation at pole-planting box impact. A simple example of such an air spring was shown in Fig. 2.13. The spring should

²The kinetic energy in upward direction is calculated with $\frac{1}{2}m_1\dot{Y}_1^2 + \frac{1}{2}m_2\dot{Y}_2^2$. The two terms represent the kinetic energy of the two athlete segments

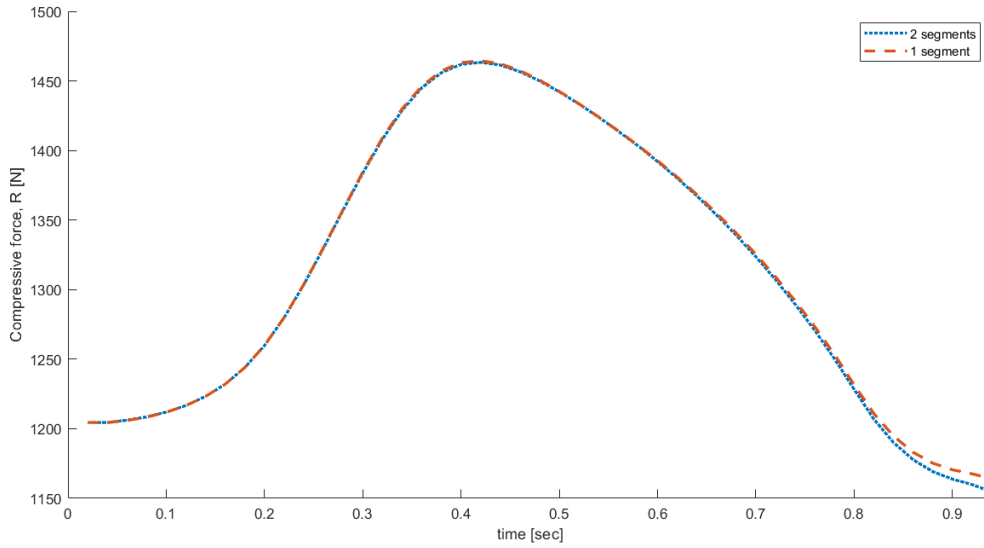


Figure 4.5: The compressive force R during 2 simulated vaults. A 1-segment pole is used for one vault and a 2-segment pole, consisting of the same properties, is used for the other vault.

have a relatively high bending stiffness, to reduce the amount friction. In the mechanical model the spring can be modeled as a pole segment. The length of this segment will vary during the vault, as the spring contracts and expands. A differential equation was derived in Section 2.5.2.4 which describes the motion of the spring. For convenience, the equation is repeated here.

$$N(t) - A \left[\left(\frac{L_0}{L_0 - x(t)} \right)^Y P_0 - P_{atm} \right] = m \frac{d^2 x}{dt^2} \quad (4.1)$$

The normal force N can be calculated with:

$$N(t) = R \cos \theta \quad (4.2)$$

Even though the spring segment should be much stiffer than the other segments, it will still slightly bend. So θ will not be equal at the segment ends. The average θ of the two ends will be used.

The 2nd order differential equation is solved iteratively, using Euler's method. Eq. 4.1 is discretized and split into two 1st order differential equations.

$$x_{i+1} = x_i + dt \cdot v_i \quad (4.3a)$$

$$v_{i+1} = v_i + dt \frac{1}{m} \left[N_i - A \left(\left(\frac{L_0}{L_0 - x_i} \right)^Y P_0 - P_{atm} \right) \right] \quad (4.3b)$$

Here x is the spring displacement and v is the velocity of the spring. If the velocity v is positive the spring is contracting. The spring is expanding when v is negative. The spring displacement and velocity is zero at $t = t_0$.

A vault with axial spring is simulated. This is shown in Fig. 4.6. The spring response is shown in Fig. 4.7.

Approximately 10% of the energy generated during the run-up phase is lost during impact. This is equal to around 50 cm of height.

About 10% of the energy that is stored in an air spring is lost due to friction. Assuming that only 5% of the initial kinetic energy is dissipated at impact when an axial spring is used, the total loss of height is approximately a 32 cm lower vault. This shows that an axial spring could improve pole vault performance. If the losses due to friction can be reduced, an axial spring will be more appealing.

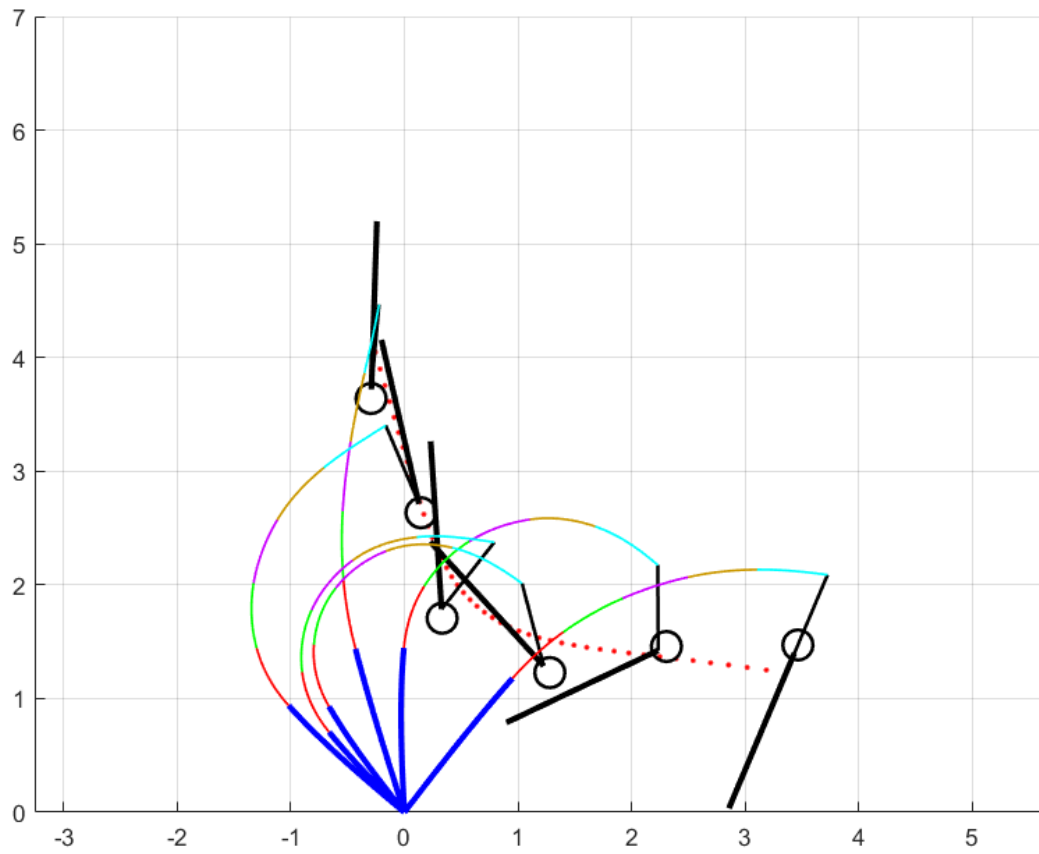


Figure 4.6: Vault with an axial spring

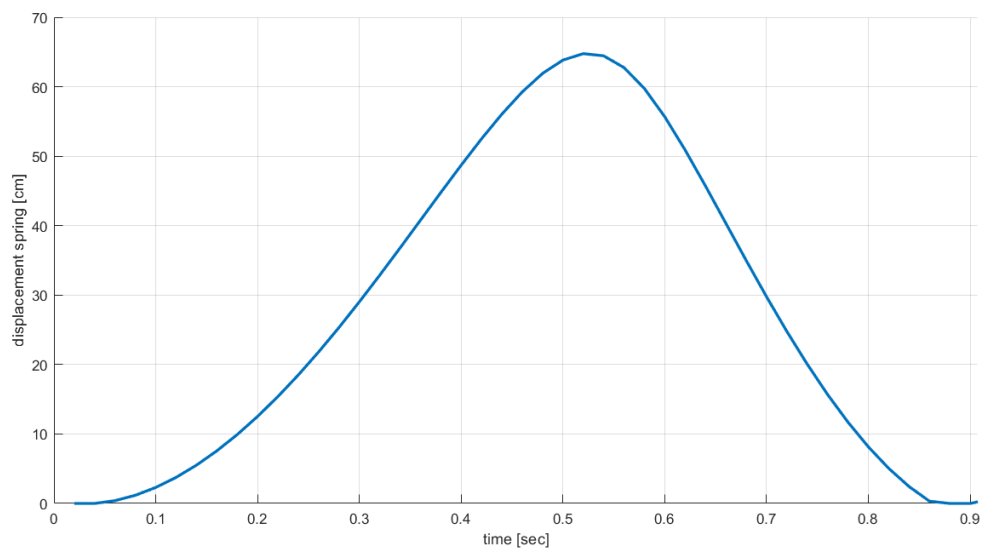


Figure 4.7: Spring response

5

Optimization

Pole vaulting is extremely complex. As discussed earlier, three factors influence a vault.

- The initial conditions
- The system properties
- The control torques

Pole vault performance depends on these factors. Therefore, it is important to explore which of these factors can be optimized.

The initial conditions are the general coordinates and their time derivatives at t_0 . The vaulter tries to increase his kinetic energy as much as possible, while carrying the pole. The run-up velocity should be maximized.

The system properties can be split into athlete- and pole properties. It is assumed that the athlete properties are fixed. The spring properties are also considered as part of the pole properties. The pole properties are very important in terms of vault performance and should be optimized for each vault.

Lastly, the control torques also greatly influence the vault. [Reijne \(2016\)](#) obtained the control torques for a constant stiffness pole by trial and error. The acquired control torques are shown in [Fig. 5.1](#). The corresponding vault was shown earlier in [Fig. 3.4](#).

[Section 5.1](#) will explain the optimization scheme that was used to optimize the control torques for various variable stiffness poles. Finding the favorable axial spring properties will be discussed in [Section 5.2](#).

5.1. Control torques

An optimization scheme is used to optimize the control torques. This scheme is based on the work of [van den Bosch \(2018\)](#). In MATLAB the pre-programmed function 'fmincon' is used to optimize the control strategy. The solver command in MATLAB looks as follows:

$$x = \text{fmincon}(\text{fun}, x_0, [], [], [], [], \text{lb}, \text{ub}, \text{nonlcon}) \quad (5.1)$$

The function 'fmincon' finds the minimum of a problem iteratively. During each iteration a complete vault is simulated. In [Eq. 5.1](#) x_0 is the initial guess for the control torques during the first vault. The

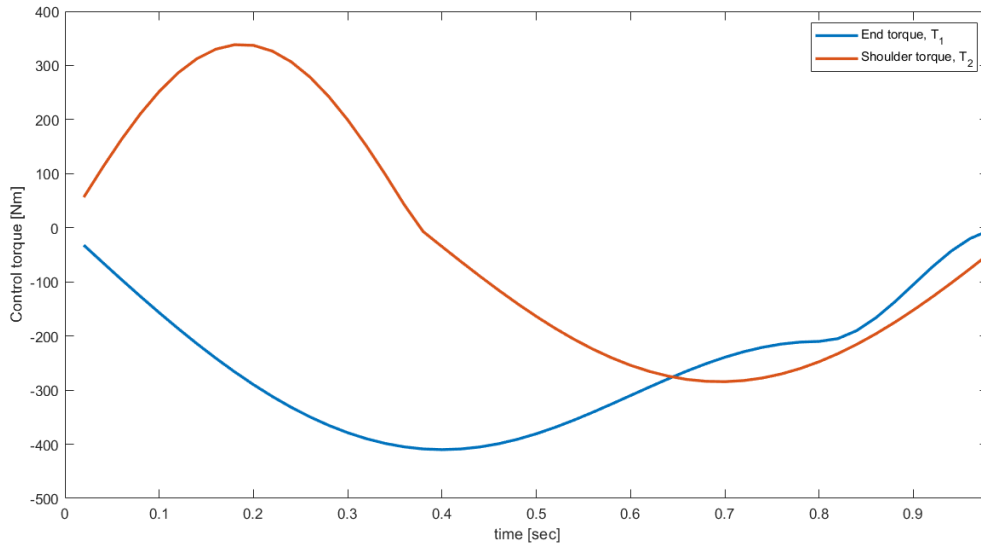


Figure 5.1: Control torques obtained by trial and error (Reijne, 2016)

control torques are given by a 6th degree polynomial, as a function of time.

$$T_1 = At^6 + Bt^5 + Ct^4 + Dt^3 + Et^2 + Ft + G \quad (5.2a)$$

$$T_2 = Ht^6 + It^5 + Jt^4 + Kt^3 + Lt^2 + Mt + N \quad (5.2b)$$

The initial guess x_0 is an array containing the constants A to N , so $x_0 = [A, B, \dots, N]$. The hand torques and shoulder torques are given by T_1 and T_2 , respectively.

In Eq. 5.1 fun is the objective function that should be minimized. At the end of each iteration, which is also the end of a vault, the energy is determined by calculating the potential energy based on the center of mass and adding the kinetic energy in upward direction. This is done as follows:

$$E_{end} = (m_1 + m_2)g \frac{m_1 Y_{cm,1} + m_2 Y_{cm,2}}{m_1 + m_2} + \frac{1}{2} m_1 \dot{Y}_1^2 + \frac{1}{2} m_2 \dot{Y}_2^2 \quad (5.3)$$

Here the first term is the potential energy. The second and third term are the kinetic energy in upward direction of the first and second athlete segment. The velocity of the second segment can be calculated with the transformation matrix T (Appendix A). The energy is calculated in this manner, as these terms contribute to the final obtained height. As 'fsolve' is a minimization algorithm, the energy equation is multiplied by -1 .

In Eq. 5.1 lb and ub represent the lower and upper boundaries of the constants A to N . In $nonlcon$ the vault is simulated as well, just as in the objective function. Here the constraints are checked. E.g. the final X position of the vaulter should be between 0 and -80 cm, which is the region for the placing the bar. Also the joints of the athlete are constrained, to prevent hyper flexing or hyper extension.

In this way optimization is done for three poles. The initial conditions are given in Table 4.4. The athlete properties are given in Table 4.3. The pole properties are given in Table 5.1. As can be seen pole 1 is a constant stiffness pole. Pole 2 and 3 are stiff at one end and soft at the other end. Pole 2 is soft at the end where the vaulter holds on to the pole and pole 3 is just the opposite. The control torques are optimized for the three poles. The optimized control torques are shown in Fig. 5.2 The control torques are very alike, even though the stiffness distribution of the three pole is very different. The control strategy is different, compared to the control strategy shown in Fig. 5.1. A positive torque T_1 is used after $t = 0.55$ sec. This will be discussed in Section 6.1.

The vaults for the three poles are very similar, in terms of forces and flight path. The deformation of the pole during the vault is not the same for the three poles, as expected. In Fig. 5.3 the vault at

Table 5.1: Pole properties of three poles, for which the control torques are optimized

	pole 1	pole 2	pole 3
Pole length, L	4.57 m	4.57 m	4.57 m
Length segments, L_i	$1/2L, 1/2L$	$1/4L, 1/4L, 1/4L, 1/4L$	$1/4L, 1/4L, 1/4L, 1/4L$
Global stiffness, B_0	$2522 N \cdot m^2$	$2280 N \cdot m^2$	$2280 N \cdot m^2$
Stiffness segments, B_i	$1B_0$	$3B_0, 1.5B_0, 0.9B_0, 0.6B_0$	$0.6B_0, 0.9B_0, 1.5B_0, 3B_0$

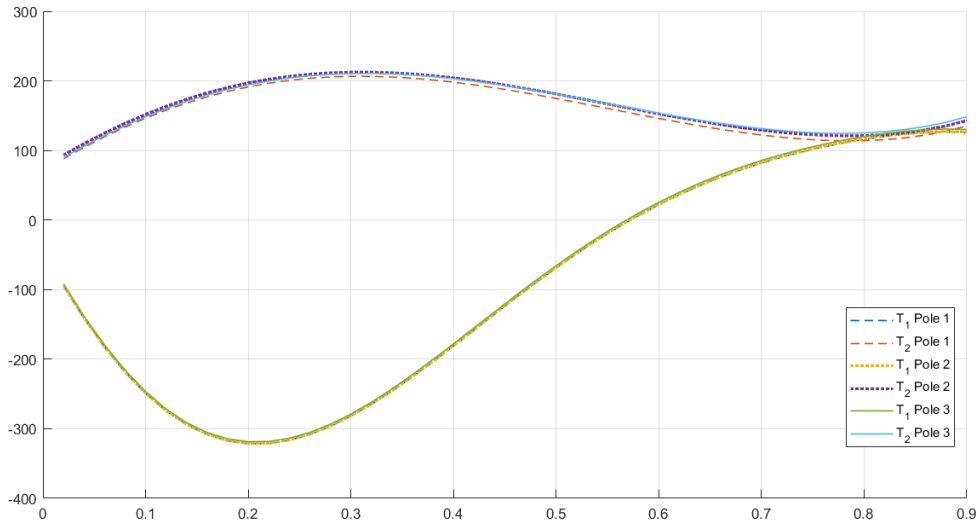


Figure 5.2: Optimized control torques

$t = 0.22 \text{ sec}$ is shown. Clearly the difference in pole deformation can be seen. The constant stiffness pole deforms homogeneous, unlike the variable stiffness poles. It can be noticed that the flight path is equal for the three poles up to $t = 0.22 \text{ sec}$. This also applies for the remainder of the vault. The total obtained height is 6.94 m for pole 1, 6.87 m for pole 2 and 6.82 m for pole 3.

5.2. Axial spring

The right spring properties for a given vaulter and set control torques can be easily found with trial and error. The response of the air spring depends on the spring dimensions, the type of air inside the spring, the ambient pressure and the preforce. The type of air is of little influence. Normal air is used for simulations, having a specific heat capacity of $1005 \frac{\text{kJ}}{\text{kg} \cdot \text{K}}$ and molar mass of $28.97 \text{e} - 3 \text{ kg/mol}$. A value of 101325 Pa is used for the ambient air pressure. The spring response can be tailored by changing the spring dimensions and preforce. The preforce depends on the initial pressurization of the air inside the spring. It is given by:

$$F_i = (P_i - P_0)A \quad (5.4)$$

A vault is simulated, using the spring properties given in Table 5.2. The spring clearly contracts and expands. However, at the end of the vault the spring seems to contract again. This spring response is not as desired. is shown in Fig. 5.4. This results in a lower obtained height. The energy at the end of the vault is 4041 J. The obtained height is 5.88 m.

The response is too fast. The spring should be back in its initial state at the exact end of the vault.

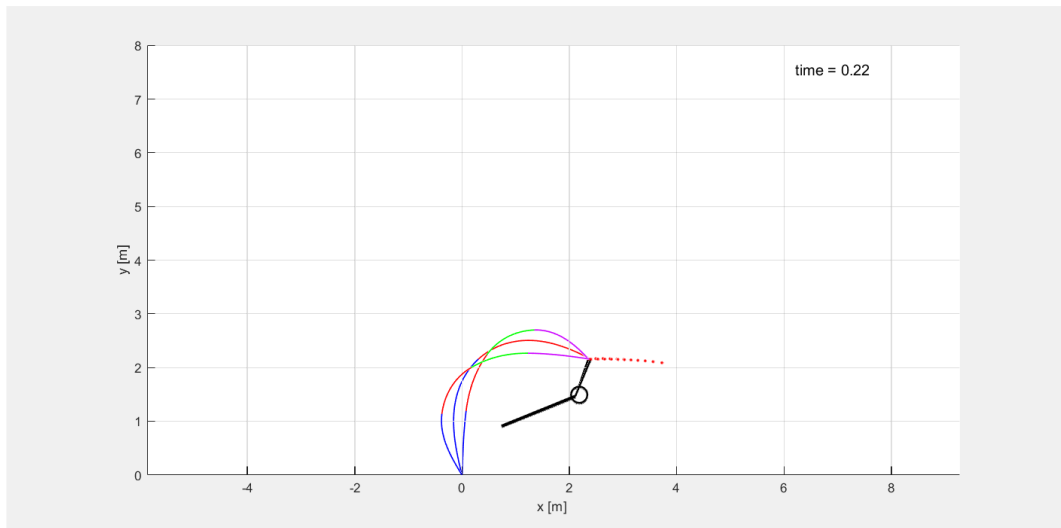


Figure 5.3: Vault at $t = 0.22 \text{ sec}$ for three different poles

Table 5.2: Input parameters for a variable stiffness pole

Initial length, L_i	0.8 m
Diameter, D	4 cm
Cross-sectional area, A	12.6 cm ²
Mass, m	70 kg
Initial pressure, P_i	1.79 atm
Preforce, F_i	100 N

Then it has returned all energy back to the vaulter. This can be done by either using a larger initial length. The vault is simulated again, now using a preforce of 200 N instead of 100 N. The spring response is shown in Fig. 5.5. This spring response is perfect. The energy at the end of the vault is 4857 J. The obtained height is 7.07 m. The simulated vault is shown in Fig. 5.6.

The axial spring can also be placed at other locations on the pole. However, the simulated vaults are not feasible then. When the spring is placed at the opposite end, at the location where the vaulter holds on to the pole, the normal force changes too much during the vault. This makes it impossible to get the right spring response. If the axial spring is placed in the middle of the pole, the spring will bend too much. This increases the friction and this location is therefore also not desired.

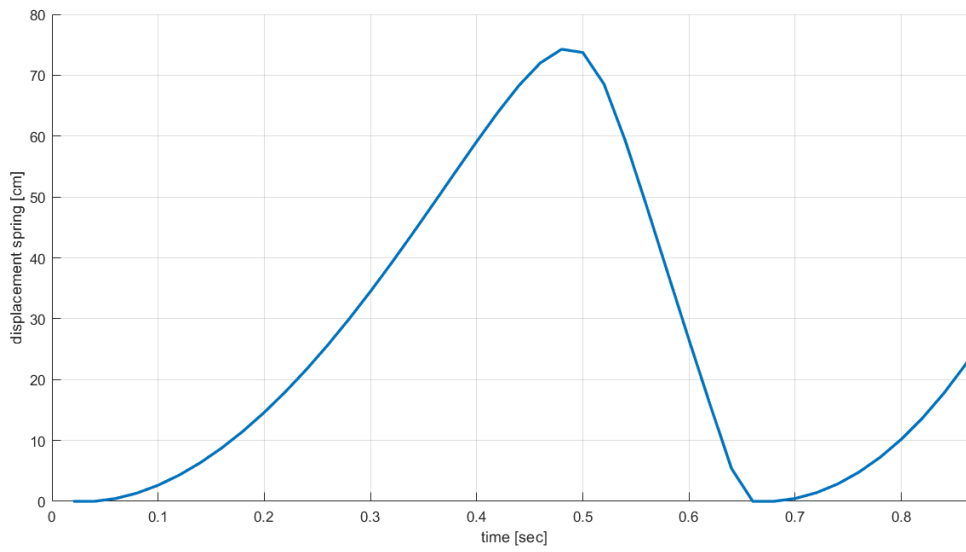


Figure 5.4: Undesired spring response

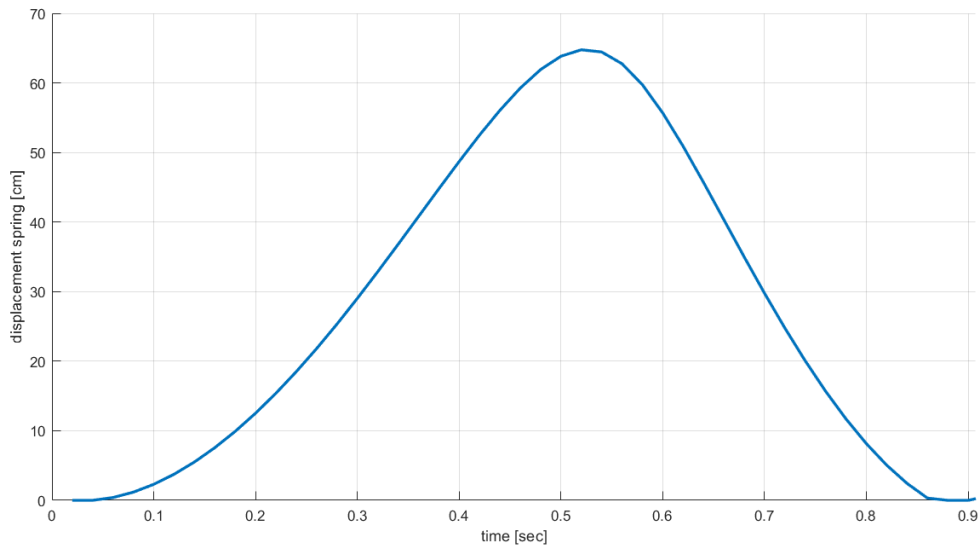


Figure 5.5: Desired spring response

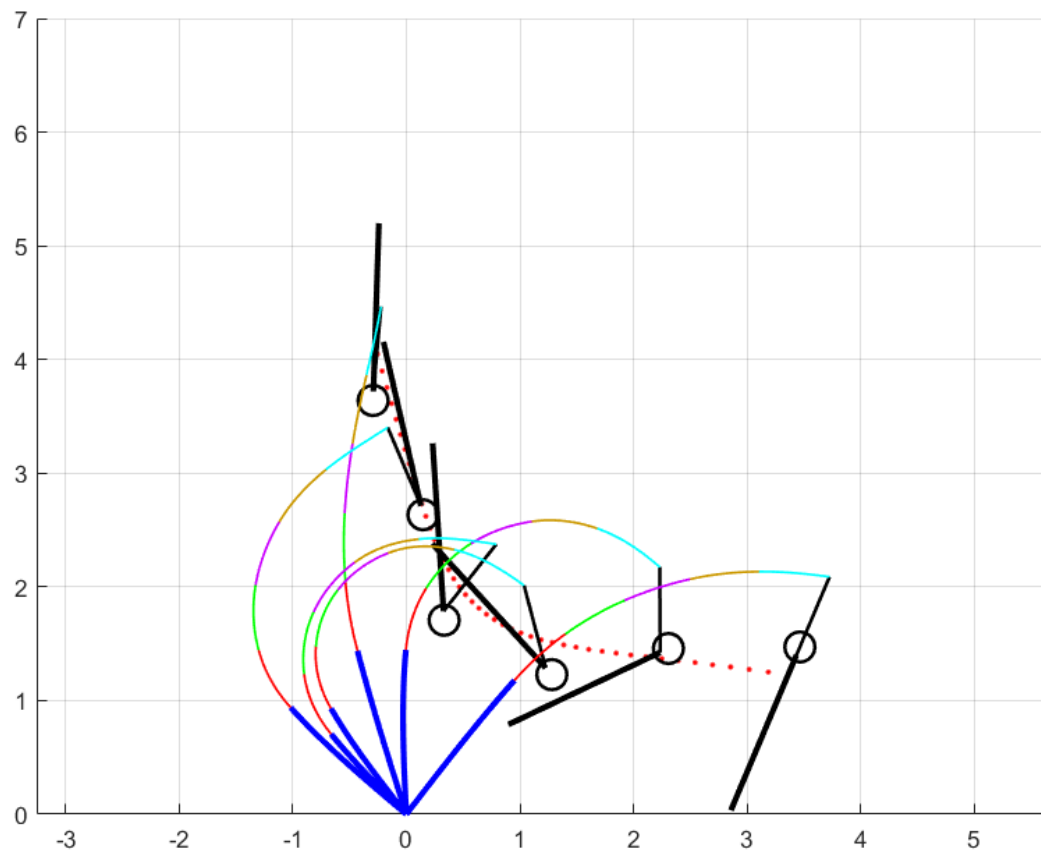


Figure 5.6: Desired spring response

6

Discussion

This chapter will discuss limitations and simplifications of the analytical model, as well as other notable observations of the analytical model.

[Section 6.1](#) will treat the deformation of pole subjected to a negative end torque. In [Section 6.1](#) the error in pole length or segment lengths will be shown. Other limitations and simplifications of the model will be discussed in [Section 6.3](#).

6.1. Opposite applied torque

Optimization the control torques showed that it was desired to apply a positive torque during the pole straightening phase. During pole bending the vaulter can store more energy into the pole by applying a negative torque. This is done by pulling with the hand at the pole end and pushing with the other hand. After MPB the vaulter can help straightening of the pole by doing just the opposite. This is showed in [Fig. 6.1](#)

Solving the compressive force and deformation of a vaulting pole is done by looking at a fictitious pole or fictitious poles, in case of a variable stiffness pole ([Section 3.2](#)). This was shown in [Fig. 3.2](#). The fictitious pole is cut somewhere. At this cut the internal moment should be equal to end torque applied on the real pole. Optimization of the control torques did give positive end torques in some cases. However, the internal moment can never be positive for the imaginary case. It is therefore important to look at the elastica solution when applying a positive end torque, and verify that the solution is correct.

The deformation of a variable stiffness pole is examined. A positive end torque is applied. The input parameters are given in [Table 6.1](#). The deformed pole is shown in [Fig. 6.2](#). The compressive force R is found to be -1400 N .

Firstly, it should be noticed that the pole in [Fig. 6.2](#) is deformed in the shape of an 's'. Its curvature changes direction after going through the pole's x axis. This shape is logical, as the compressive force bends the pole in one direction, but at the pole end the applied end torque tries to bend the pole in the other direction. Furthermore, the same shape is found the research of [Fukushima et al. \(2013\)](#).

Secondly, the compressive force R is examined. The same pole is used, but the end torque T is varied. For each end torque the compressive force is found by the solver. The outcome is given in [Table 6.2](#) Clearly, a linear relation between the end torque T and compressive force R can be observed. The obtained values for R are realistic, when going from a negative to a positive end torque. It is therefore assumed that the elastica solutions for positive end torques are correct.

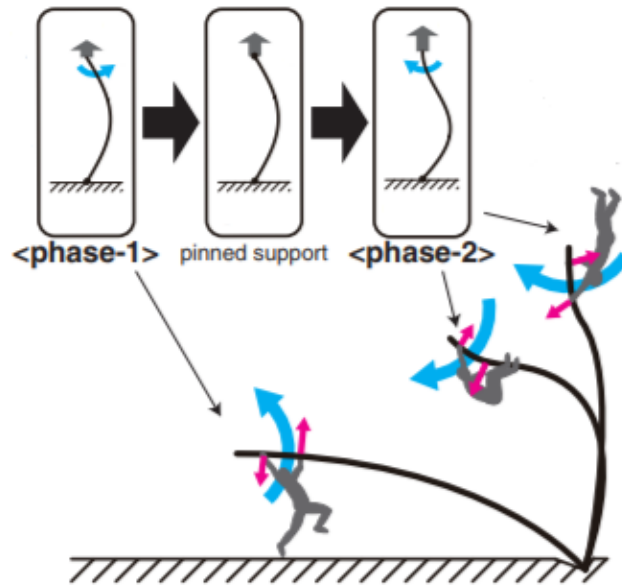


Figure 6.1: Apply an end torque during pole bending and an opposite end torque during pole straightening (Fukushima *et al.*, 2013)

6.2. Segment length discrepancy

When solving the compressive force R and the angle γ , the amplitude angle ϕ has to be determined several times, at different locations on the pole. This can be seen in [Appendix F](#). Knowing the length of segment 1, the amplitude angle of at the connection between segment 1 and 2 is calculated with:

$$\phi_1 = \pi \frac{L_1}{L_{fic,1}} - \frac{\pi}{2} \quad (6.1)$$

[Eq. 6.1](#) assumes a linear relation between the amplitude angle and the ratio $\frac{L_1}{L_{fic,1}}$, while this is not the case. Therefore the amplitude angle will be an approximation, resulting in a small error for the segment length.

The amplitude angle can be determined exactly. The arc length is given by ([Appendix B.1](#)):

$$s = \sqrt{\frac{B}{R}} K(k, \phi) \quad (6.2)$$

Knowing s , B , R , and k , the amplitude angle ϕ can be determined with the pre-programmed function 'jacobIAM' in MATLAB. The function will numerically solve for ϕ . During a vault ϕ has to be determined hundreds of times. Solving ϕ exactly will slow the simulation significantly.

The error in segment lengths is checked for a deformed pole. The error in segment lengths will also result in an error in the compressive force R . The pole is subjected to an end torque T of -500 Nm . The pole chord l is 3.5 m . The total pole length L is 4.57 m . The segment stiffnesses and lengths are shown in [Table 6.3](#). The compressive force R is 1124 N for the approximate lengths and 1112 N for the exact segment lengths.

6.3. Other limitations and simplifications

Other limitations and simplifications of the mechanical model are shown below.

Table 6.1: Input parameters for a variable stiffness pole, subjected to a positive end torque

Pole length, L	4.57 m
Length segment 1, L_1	$1/3L$
Length segment 2, L_2	$1/3L$
Length segment 3, L_3	$1/3L$
Chord length, l	3.6 m
Global stiffness, B_0	$2522 N \cdot m^2$
Stiffness segment 1, B_1	$0.6B_0$
Stiffness segment 2, B_2	$0.8B_0$
stiffness segment 3, B_3	$1B_0$
End moment, T	$800 N \cdot m$

Table 6.2: Relation between end torque T and compressive force R for a pole with properties given in Table 6.1

End torque, T	Compressive force, R	ΔR
$-300 N \cdot m$	$-906 N$	-
$-200 N \cdot m$	$-950 N$	44 N
$-100 N \cdot m$	$-994 N$	44 N
$0 N \cdot m$	$-1038 N$	44 N
$100 N \cdot m$	$-1082 N$	44 N
$200 N \cdot m$	$-1127 N$	45 N
$300 N \cdot m$	$-1171 N$	44 N

- The hand torques and shoulder torques are constraint. In reality these torques are motion dependent. The power should be constrained, which is the torque multiplied with the rotational velocity.
- The mass moment of inertia is constant, while this is changing during the vault in reality.
- Only two segments are used to model the vaulter. Rotation of the hips is prohibited. This is also a shortcoming.
- The model is $2d$, instead of $3d$. However the forces and moments outside the xy plane are small and can be neglected.
- Impact is not taken into account.

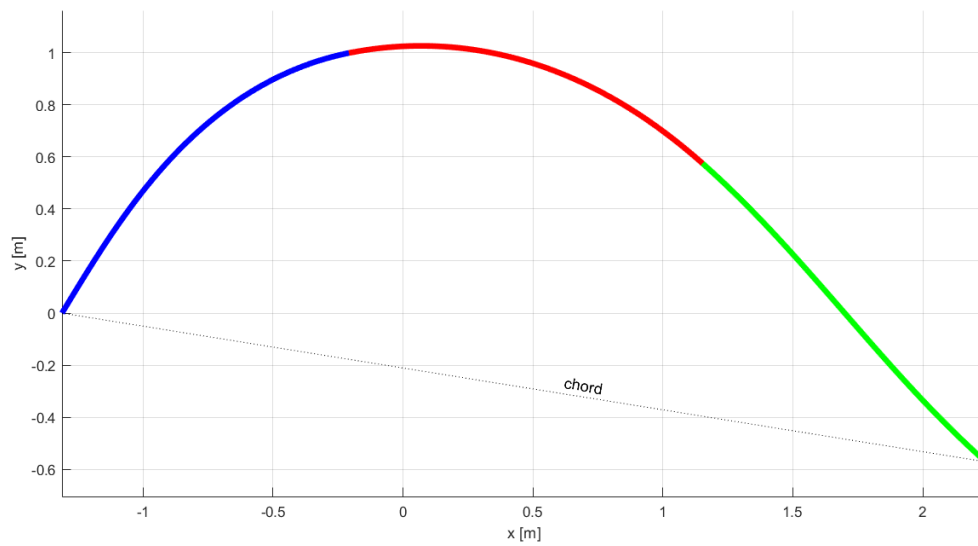


Figure 6.2: Elastica solution for a variable stiffness pole. The input properties are given in Table 6.1. The applied end torque is positive.

Table 6.3: Segment properties and differences

Segment	1	2	3
Stiffness, B_n	$2B_0$	$1.5B_0$	$1B_0$
Real Length	$1/6L$	$1/6L$	$1/6L$
Approximated Length	0.8104 m	0.7671 m	0.7239 m
Difference	6.4%	0.7%	-5.0%
Segment	4	5	6
Stiffness, B_n	$0.9B_0$	$0.8B_0$	$0.5B_0$
Real Length	$1/6L$	$1/6L$	$1/6L$
Approximated Length	0.7117 m	0.7371 m	0.7854 m
Difference	-6.6%	-3.2%	3.1%

7

Conclusions and Recommendations

The conclusions of this research have been summarized and are shown below.

- An analytical model has been developed with which a vault can be simulated. A pole having a variable stiffness over its length can be used in this model. A longitudinal spring can also be added to the pole, at any location.
- Vaults with variable stiffness poles are realistic. The forces during the vault and flight path of the athlete are comparable to real vaults.
- An optimization scheme is used to examine the optimal control torque and the optimal stiffness distribution. Optimizing only the control torques is tedious, because the control strategy is highly dependent on the pole properties, and vice versa.
- The control torques are optimized, keeping the stiffness distribution constant. This has been done for three poles having different stiffness distributions. The first pole had a constant stiffness along the length of the pole. The second pole was very stiff near the top of the pole, the stiffness decreased gradually towards the other end. The third pole was just the opposite of the second pole, soft at the top and stiff at the other end. After finding the optimal control strategy, the three poles showed no significant difference in obtained height or flight path.
- A pole being stiff near the top and soft at its other end, could be better compared to a constant stiffness pole, because of a lower carry weight. The pole would be heavier near the top but much lighter near the other end. A lower carry weight would result in a higher run up velocity by the vaulter, consequently more energy would be generated during the run-up phase and this would increase vault performance.
- Adding an axial spring to the pole shows promising results. The simulation shows a realistic vault, similar to current vaults. The optimized spring properties are realistic as well. It is assumed that using a longitudinal spring, less energy will be dissipated during impact.

The following research question was defined, prior to the research:

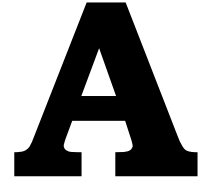
What would be the optimal material properties and optimal design for the pole vaulting pole in terms of obtainable height of the vaulter, especially in relationship with jumping technique and bio-mechanical factors of the athlete?

This question cannot be answered yet. The jumping technique (control torques), bio-mechanical factors of the athlete (athlete properties and initial conditions) and pole properties are highly dependent

on each other. This research shows that a variable stiffness pole with axial spring could improve pole vaulting performance.

The following recommendations are made.

- The athlete properties and initial conditions are set. The pole properties and control strategy is critical for a successful vault. Finding a method to optimize the torque profile and stiffness distribution simultaneously, could greatly improve pole vaulting performance.
- The axial spring should be designed in more detail. Loss of energy due to friction should be minimized.
- The current production method limits the design of the pole. An alternative manufacturing method should be developed. Two alternative production processes are shown in [Appendix G](#).
- The mass moment of inertia during a vault is now constant. In reality this is not the case. Updating this in the mechanical model will make it more realistic.
- More athlete segments should be added. The vaulter should consist of at least 3 segments. Rotation of the hips and the control torques at this hinge are important to generate a realistic vault simulation.
- The layup of the pole should be determined. Also the carry weight should be minimized.
- The spring-pole assembly should be investigated.



Derivation of the equations of motion

The athlete is modelled as two bodies, each having three degrees of freedom. They can translate in the X or Y direction, or they can rotate about the Z axis. These degrees of freedom are placed into a vector x_i .

$$x_i = \begin{bmatrix} X_{cm1} \\ Y_{cm1} \\ \phi \\ X_{cm2} \\ Y_{cm2} \\ \phi + \theta \end{bmatrix} \quad (\text{A.1})$$

According to Newton

$$\sum f_i = M_{ij} \ddot{x}_i \quad (\text{A.2})$$

Here the mass matrix is

$$M_{ij} = \begin{bmatrix} m_1 & & & & & \\ & m_1 & & & & \\ & & I_1 & & & \\ & & & m_2 & & \\ & 0 & & & m_2 & \\ & & & & & I_2 \end{bmatrix} \quad (\text{A.3})$$

The force vector contains all forces and moments on each degree of freedom.

As stated in [Section 3.1](#), only four independent generalized coordinates are needed to define the motion and position of the athlete during a vault. The independent generalized coordinates are shown in q_j

$$q_j = \begin{bmatrix} X_{cm1} \\ Y_{cm1} \\ \phi \\ \theta \end{bmatrix} \quad (\text{A.4})$$

The degrees of freedom shown in [Eq. A.1](#) can be expressed in the generalized coordinates as follows

$$g_i = \begin{bmatrix} X_{cm1} \\ Y_{cm1} \\ \phi \\ X_{cm1} - l_2 \sin(\phi) - l_3 \sin(\phi + \theta) \\ Y_{cm1} - l_2 \cos(\phi) - l_3 \cos(\phi + \theta) \\ \phi + \theta \end{bmatrix} \quad (\text{A.5})$$

The velocities \dot{x}_i can also be described in terms of the generalized coordinates

$$\dot{x}_i = \frac{\partial g_i}{\partial q_k} \dot{q}_k \quad (\text{A.6})$$

Here the term $\frac{\partial g_i}{\partial q_k}$ is the transformation matrix, which is given by

$$T_{ik} = \frac{\partial g_i}{\partial q_k} = \begin{bmatrix} 1 & 0 & 0 & 0 \\ 0 & 1 & 0 & 0 \\ 0 & 0 & 1 & 0 \\ 1 & 0 & -l_2 \cos(\phi) - l_3 \cos(\phi + \theta) & -l_3 \cos(\phi + \theta) \\ 0 & 1 & l_2 \sin(\phi) + l_3 \sin(\phi + \theta) & l_3 \sin(\phi + \theta) \\ 0 & 0 & 1 & 1 \end{bmatrix} \quad (\text{A.7})$$

The acceleration, in terms of generalized coordinates, can be derived in a similar way.

$$\ddot{x}_i = \frac{\partial g_i}{\partial q_l} \ddot{q}_l + \frac{\partial^2 g_i}{\partial q_m \partial q_p} \dot{q}_m \dot{q}_p \quad (\text{A.8})$$

Note that the term $\frac{\partial g_i}{\partial q_l}$ is equal to the transformation matrix T_{ik} , that converts the velocities \dot{q}_k to \dot{x}_i . The second term in Eq. A.8 is usually addressed to as the convective acceleration, h_i .

$$h_i = \begin{bmatrix} 0 \\ 0 \\ 0 \\ l_3 \dot{\phi}^2 \sin(\phi + \theta) + l_3 \dot{\theta}^2 \sin(\phi + \theta) + l_2 \dot{\phi}^2 \sin(\phi) + 2l_3 \dot{\phi} \dot{\theta} \sin(\phi + \theta) \\ l_3 \dot{\phi}^2 \cos(\phi + \theta) + l_3 \dot{\theta}^2 \cos(\phi + \theta) + l_2 \dot{\phi}^2 \cos(\phi) + 2l_3 \dot{\phi} \dot{\theta} \cos(\phi + \theta) \\ 0 \end{bmatrix} \quad (\text{A.9})$$

Consequently, Eq. A.8 can be rewritten as

$$\ddot{x}_i = T_{ij} \ddot{q}_j + h_i \quad (\text{A.10})$$

Newton's law (Eq. A.2) can be rewritten in the d'Alembert form.

$$\sum f_i - M_{ij} \ddot{x}_i = 0 \quad (\text{A.11})$$

Introducing the fictitious force $M_{ij} \ddot{x}_i$, this changes the dynamic situation into a static situation. Adding the virtual velocities $\delta \dot{x}_i$ gives the virtual power equation.

$$\delta \dot{x}_i (\sum f_i - M_{ij} \ddot{x}_i) = 0 \quad (\text{A.12})$$

The virtual velocities and the accelerations can be transformed to independent coordinates, using the transformation matrix.

$$T_{ik} \delta \dot{q}_k (\sum f_i - M_{ij} (T_{jl} \delta \ddot{q}_l + h_j)) = 0 \quad (\text{A.13})$$

The virtual velocities of the generalized coordinates $\delta \dot{q}_j$ are independent so every k equation must be zero as in

$$T_{ik} (\sum f_i - M_{ij} (T_{jl} \delta \ddot{q}_l + h_j)) = 0 \quad (\text{A.14})$$

Rearranging gives

$$T_{ik} M_{ij} T_{jl} \ddot{q}_l = T_{ik} \sum (f_i + T_{ik} M_{ij} h_j) \quad (\text{A.15})$$

The force vector f_i contains the internal and external forces. The internal forces are gravity and the forces exerted on the athlete from the pole. The internal forces are given by

$$f_i = \begin{bmatrix} R_n \cos(\lambda) + R_t \sin(\lambda) \\ R_n \sin(\lambda) + R_t \cos(\lambda) - m_1 g \\ l_1 R_n \cos(\phi + \lambda) + l_1 R_t \sin(\phi + \lambda) \\ 0 \\ -m_2 g \\ 0 \end{bmatrix} \quad (\text{A.16})$$

The external forces are the control torques applied by the athlete, which do not have to be transformed.

$$y = \begin{bmatrix} 0 \\ 0 \\ -T_1 \\ T_2 \end{bmatrix} \quad (\text{A.17})$$

Substituting these expressions into [Eq. A.15](#) gives the final system of equations of motion.

$$T_{i,k} M_{ij} T_{j,l} \ddot{q}_l = y_l + T_{i,k} \sum (f_i + T_{i,k} M_{ij} g_j) \quad (\text{A.18})$$

B

Derivation of the arc length and curve shape

This Appendix shows the derivation of the arc length and curve shape for a slender rod with constant bending stiffness B , subjected to an end force only as shown in Fig. B.1, undergoing very large elastic deformation (elastica theory).

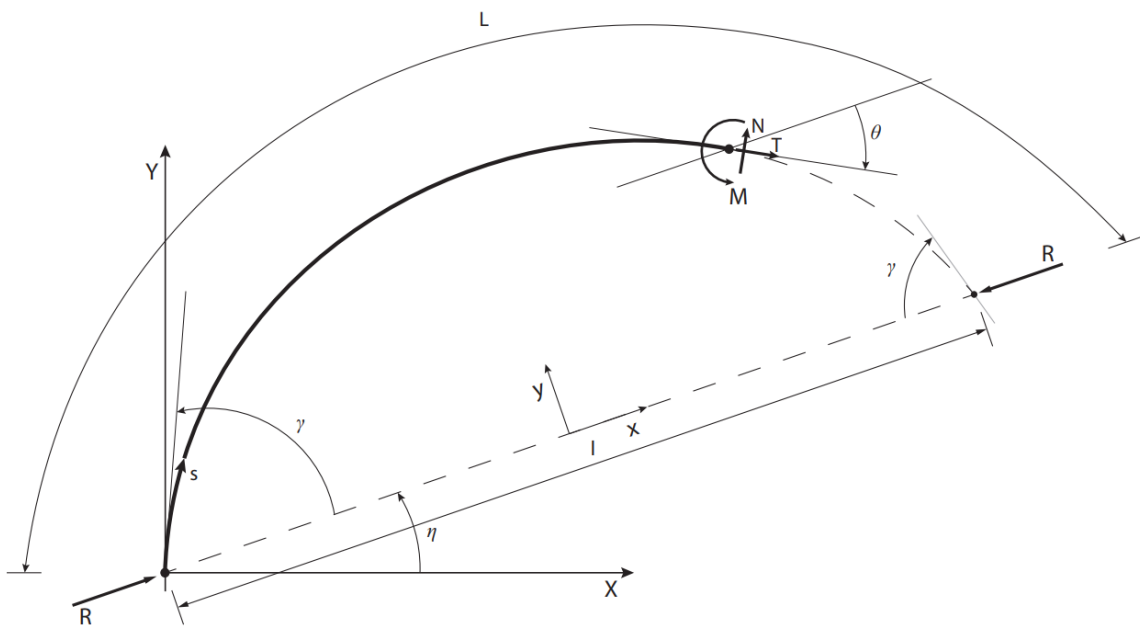


Figure B.1: Schematic diagram of a fictitious pole subjected to an end force only (Reijne, 2016)

B.1. Arc length

The equilibrium equations can be established from the cutting point.

$$T = -R \cos \theta \quad (\text{B.1a})$$

$$N = -R \sin \theta \quad (\text{B.1b})$$

$$\frac{dM}{ds} + N = 0 \quad (\text{B.1c})$$

The bending moment is assumed to be linear with respect to the curvature.¹

$$M = -B \left(\frac{d\theta}{ds} \right) \quad (\text{B.2})$$

This expression for M is substituted in Eq. B.1c and solved for N .

$$N = B \left(\frac{d^2\theta}{ds^2} \right) \quad (\text{B.3})$$

This in turn can be substituted in the normal force equation, Eq. B.1b, which gives after rearranging:

$$B \left(\frac{d^2\theta}{ds^2} \right) + R \sin \theta = 0 \quad (\text{B.4})$$

To obtain an expression for ds , this equation is integrated with respect to θ .²

$$\frac{1}{2} B \left(\frac{d\theta}{ds} \right)^2 - R \cos \theta = C \quad (\text{B.5})$$

where C is a constant. As shown in Fig. 3.3, at the global origin where $s = 0$, the tangent θ is equal to γ . Using this boundary condition, Eq. B.5 can be solved for C .

$$C = -R \cos \theta \quad (\text{B.6})$$

Substituting in Eq. B.5 and rearranging gives:

$$\left(\frac{d\theta}{ds} \right)^2 = \frac{2R}{B} (\cos \theta - \cos \gamma) \quad (\text{B.7})$$

Next, Eq. B.7 is rewritten using the double angle formula³.

$$\left(\frac{d\theta}{ds} \right)^2 = \frac{4R}{B} \left(\sin \frac{1}{2}\gamma - \sin \frac{1}{2}\theta \right) \quad (\text{B.8})$$

As shown in Section 3.2, the arguments γ and θ can be written in terms of the modulus k and amplitude angle ϕ . For convenience, these relations are repeated here.

$$k = \sin \frac{1}{2}\gamma \quad (\text{B.9a})$$

$$\sin \phi = \frac{\sin \frac{1}{2}\theta}{\sin \frac{1}{2}\gamma} \quad (\text{B.9b})$$

Using the above-mentioned relations, Eq. B.8 is rewritten in terms of k and ϕ .

$$\left(\frac{d\theta}{ds} \right)^2 = \frac{4R}{B} (k^2 - k^2 \sin^2 \phi) \quad (\text{B.10})$$

Solving for $\frac{d\theta}{ds}$

$$\frac{d\theta}{ds} = \frac{R}{B} 2k \sqrt{1 - \sin^2 \phi} \quad (\text{B.11})$$

¹For large deflections, the curvature is equal to $\frac{d\theta}{ds}$.

²Note that by differentiating Eq. B.5 with respect to θ , indeed Eq. B.4 is obtained, as $\frac{d}{d\theta} \left[\frac{1}{2} \left(\frac{d\theta}{ds} \right)^2 \right] = \frac{d\theta}{ds} \cdot \frac{d}{d\theta} \left(\frac{d\theta}{ds} \right) = \frac{d\theta}{ds} \cdot \frac{d}{ds} \left(\frac{d\theta}{ds} \right) = \frac{d^2\theta}{ds^2}$

³ $\cos x = 1 - 2 \sin^2 \left(\frac{1}{2}x \right)$

and using the Pythagorean identity⁴ gives

$$\frac{d\theta}{ds} = \frac{R}{B} 2k \cos \phi \quad (\text{B.12})$$

Eq. B.9b is differentiated and solved for $d\theta$.

$$d\theta = \frac{2k \cos \phi}{\cos \frac{1}{2}\theta} d\phi \quad (\text{B.13})$$

The variable θ is still in there, while only terms of k and ϕ are preferred. It is left in there for now and will be replaced later.

Substitute Eq. B.13 in Eq. B.12 and rearrange.

$$\frac{d\phi}{ds} = \sqrt{\frac{R}{B}} \cos \frac{1}{2}\theta \quad (\text{B.14})$$

Again using the Pythagorean identity, Eq. B.14 becomes:

$$ds = \sqrt{\frac{B}{R}} \frac{d\phi}{\sqrt{1 - \sin^2 \frac{1}{2}\theta}} \quad (\text{B.15})$$

At this point θ is replaced by substitution of the expression shown in Eq. B.9b.

$$ds = \sqrt{\frac{B}{R}} \frac{d\phi}{\sqrt{1 - k^2 \sin^2 \phi}} \quad (\text{B.16})$$

The arc length can now be obtained by integrating Eq. B.16.

$$s = \sqrt{\frac{B}{R}} \int \frac{1}{\sqrt{1 - k^2 \sin^2 \phi}} d\phi \quad (\text{B.17})$$

The integral on the RHS is an incomplete elliptic integral of the first kind. It can be computed for the given arguments k and ϕ .

Consequently, the final form of the arc length is:

$$s = \sqrt{\frac{B}{R}} K(k, \phi) \quad (\text{B.18})$$

B.2. Curve shape

To determine the shape of the pole, an expression has to be found for the local coordinates x and y . These coordinates are also shown in Fig. B.1.

Given the tangent θ , the following relations are found when looking at an infinitesimal small part of the pole:

$$\frac{dx}{ds} = \cos \theta \quad (\text{B.19a})$$

$$\frac{dy}{ds} = \sin \theta \quad (\text{B.19b})$$

⁴ $\sin^2 x + \cos^2 x = 1$

Combining Eq. B.15 and Eq. B.19a gives

$$dx = \sqrt{\frac{B}{R}} \frac{\cos \theta}{\sqrt{1 - \sin^2 \frac{1}{2} \theta}} d\phi \quad (\text{B.20})$$

Using the double angle formula to replace $\cos \theta$ gives:

$$dx = \sqrt{\frac{B}{R}} \frac{1 - 2 \sin^2 \frac{1}{2} \theta}{\sqrt{1 - \sin^2 \frac{1}{2} \theta}} d\phi \quad (\text{B.21})$$

To get rid of θ , again Eq. B.9b is substituted in Eq. B.21.

$$dx = \sqrt{\frac{B}{R}} \frac{1 - 2k^2 \sin^2 \phi}{\sqrt{1 - k^2 \sin^2 \phi}} d\phi \quad (\text{B.22})$$

This expression is rewritten to obtain an expression for dx in terms of elliptic integrals.

$$\begin{aligned} dx &= \sqrt{\frac{B}{R}} \frac{2 - 2k^2 \sin^2 \phi - 1}{\sqrt{1 - k^2 \sin^2 \phi}} d\phi \\ &= \sqrt{\frac{B}{R}} \frac{2(1 - k^2 \sin^2 \phi) - 1}{\sqrt{1 - k^2 \sin^2 \phi}} d\phi \\ &= \sqrt{\frac{B}{R}} \frac{2\sqrt{1 - k^2 \sin^2 \phi} \sqrt{1 - k^2 \sin^2 \phi} - 1}{\sqrt{1 - k^2 \sin^2 \phi}} d\phi \\ &= \sqrt{\frac{B}{R}} 2\sqrt{1 - k^2 \sin^2 \phi} d\phi - \sqrt{\frac{B}{R}} \frac{1}{\sqrt{1 - k^2 \sin^2 \phi}} d\phi \end{aligned} \quad (\text{B.23})$$

The final expression is integrated to obtain an expression for x .

$$x = \sqrt{\frac{B}{R}} 2 \int \sqrt{1 - k^2 \sin^2 \phi} d\phi - \sqrt{\frac{B}{R}} \int \frac{1}{\sqrt{1 - k^2 \sin^2 \phi}} d\phi \quad (\text{B.24})$$

The first integral on the RHS is an incomplete elliptic integral of the second kind. The second integral is again an incomplete elliptic integral of the first kind.

Consequently, The final expression for x is:

$$x = \sqrt{\frac{B}{R}} (2E(k, \phi) - K(k, \phi)) \quad (\text{B.25})$$

The expression for the local coordinate y is found in a similar way. Combining Eq. B.15 and Eq. B.19b results in:

$$dy = \sqrt{\frac{B}{R}} \frac{\sin \theta}{\sqrt{1 - \sin^2 \frac{1}{2} \theta}} d\phi \quad (\text{B.26})$$

The double angle formula and Pythagorean theory are used to rewrite the terms in the fraction.

$$dy = \sqrt{\frac{B}{R}} 2 \sin \left(\frac{1}{2} \theta \right) d\phi \quad (\text{B.27})$$

Again Eq. B.9b is used to replace θ .

$$dy = \sqrt{\frac{B}{R}} 2k \sin(\phi) d\phi \quad (\text{B.28})$$

Integration gives the final expression for y :

$$y = -\sqrt{\frac{B}{R}} 2k \cos \phi \quad (\text{B.29})$$



Fourth order Runge-Kutta

An approximate solution has to be found for the following first order differential equation:

$$y'(t) = f(y(t), t), \quad \text{with } y(t_0) = y_0$$

The fourth order Runge-Kutta approximates the solution by using a weighted sum of the following slopes:

$$\begin{aligned}k_1 &= f(y(t_0), t_0) \\k_2 &= f\left(y(t_0) + k_1 \frac{h}{2}, t_0 + \frac{h}{2}\right) \\k_3 &= f\left(y(t_0) + k_2 \frac{h}{2}, t_0 + \frac{h}{2}\right) \\k_4 &= f(y(t_0) + k_3 h, t_0 + h)\end{aligned}$$

where h is the step size.

An estimation is then found for $y(t_0 + h)$ by taking a weighted sum of these slopes.

$$y(t_0 + h) = y(t_0) + \frac{k_1 + 2k_2 + 2k_3 + k_4}{6} h$$

D

Elastica solutions of poles having a variable stiffness

This Appendix shows various poles undergoing large deformation because of a compressive force and torque. The poles consist of segments having different stiffnesses. The solver needs the following input:

- The lengths of the pole segments. The sum of these lengths will be the total pole length.
- The stiffnesses of the pole segments. These will be expressed in terms of a defined global stiffness.
- The applied end torque.
- The pole chord. A smaller chord will result in the pole undergoing a larger deformation.

The output of the solver will be the applied compressive force R and γ_1 to γ_n . With these outputs the deformed poles can be plotted.

D.1. Different stiffness distribution

Firstly, two poles are shown. The first pole is stiff in the middle and has soft ends. The second pole is just the opposite; it is soft in the middle and has stiff ends. The inputs are shown in [Table D.1](#). The deformed poles are shown in [Fig. D.1](#) and [Fig. D.2](#). In these plots also the fictitious poles are shown.

D.2. Influence of the applied torque

Next, the deformation of two poles consisting of 6 segments is shown. The pole properties are the same for both poles. The total pole length L is 4.57 m . The global stiffness B_0 is $2522\text{ N} \cdot \text{m}^2$. The chord length l is 3.4 m . The properties for each segment is given in [Table D.2](#).

The applied torque T will be $-1000\text{ N} \cdot \text{m}$ and $1000\text{ N} \cdot \text{m}$. This value is unrealistically large, but it will clearly show how each pole deforms. A negative torque is desired during the pole bending phase. A positive torque is preferred during the pole straightening phase. The deformed poles are shown in [Fig. D.3](#) and [Fig. D.4](#). Note that the applied compressive force R is more than twice as much in case of the positive end torque. This is as expected, since the positive end torque wants to straighten the pole.

Table D.1: Input parameters for two variable stiffness poles

	Pole 1	Pole 2
Pole length, L	4.57 m	4.57 m
Length segment 1, L_1	$1/3L$	$1/3L$
Length segment 2, L_2	$1/3L$	$1/3L$
Length segment 3, L_2	$1/3L$	$1/3L$
Chord length, l	3.4 m	3.4 m
Global stiffness, B_0	$2522 N \cdot m^2$	$2522 N \cdot m^2$
Stiffness segment 1, B_1	$0.6B_0$	$3B_0$
Stiffness segment 2, B_1	$3B_0$	$0.6B_0$
Stiffness segment 3, B_1	$0.6B_0$	$3B_0$
End moment, T	$-300 N \cdot m$	$-300 N \cdot m$

Table D.2: Segment properties

Segment	1	2	3	4	5	6
Length, L_n	$1/6L$	$1/6L$	$1/6L$	$1/6L$	$1/6L$	$1/6L$
Stiffness, B_n	$2B_0$	$1.5B_0$	$1B_0$	$0.9B_0$	$0.8B_0$	$0.5B_0$

A much larger compressive force is needed to deform the pole so that the same pole chord length is obtained.

D.3. A pole consisting of a large amount of segments

If a pole is modeled having only a few segments, the change in stiffness going from one segment to the next might be quite big. If a more smoother transition is desired, more segments should be added to the pole. A pole consisting of a large amount of segments will be harder to solve. More outputs (γ_n) need to be determined and a good initial guess will be more critical. The solver will tend to diverge more often.

The deformation of a pole consisting of 16 segments is examined. The total pole length L is 4.57 m. The global stiffness B_0 is $2522 N \cdot m^2$. The chord length l is 3.6 m. The applied end torque T is $-500 N \cdot m$. The properties for each segment is given in Table D.3. The deformed pole is plotted in Fig. D.5. In Fig. D.6 the same pole is shown, including the fictitious poles.

Table D.3: Segment properties for a 16 segment pole

Segment	1	2	3	4	5	6	7	8
Length, L_n	$9/160L$	$6/160L$	$14/160L$	$16/160L$	$9/160L$	$5/160L$	$9/160L$	$2/160L$
Stiffness, B_n	$1B_0$	$1.3B_0$	$1.5B_0$	$2B_0$	$3B_0$	$2.3B_0$	$1.9B_0$	$1.5B_0$
Segment	9	10	11	12	13	14	15	16
Length, L_n	$12/160L$	$24/160L$	$15/160L$	$6/160L$	$7/160L$	$10/160L$	$5/160L$	$11/160L$
Stiffness, B_n	$1B_0$	$0.9B_0$	$0.8B_0$	$0.6B_0$	$1.1B_0$	$1.8B_0$	$3B_0$	$1B_0$

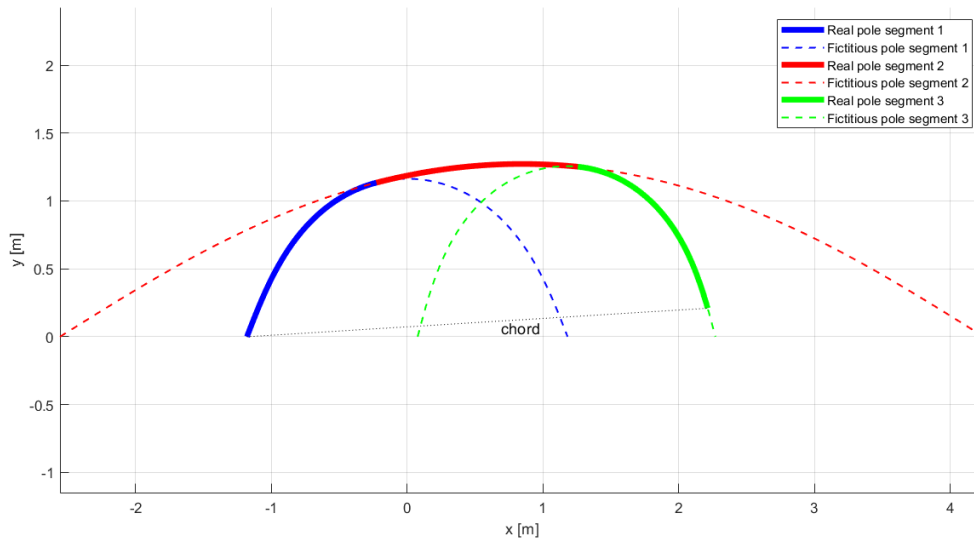


Figure D.1: Elastica solution for a pole having a high stiffness in the middle (Pole 1). The input properties are given in [Table D.1](#). The compressive end force R is found to be -1429 N.

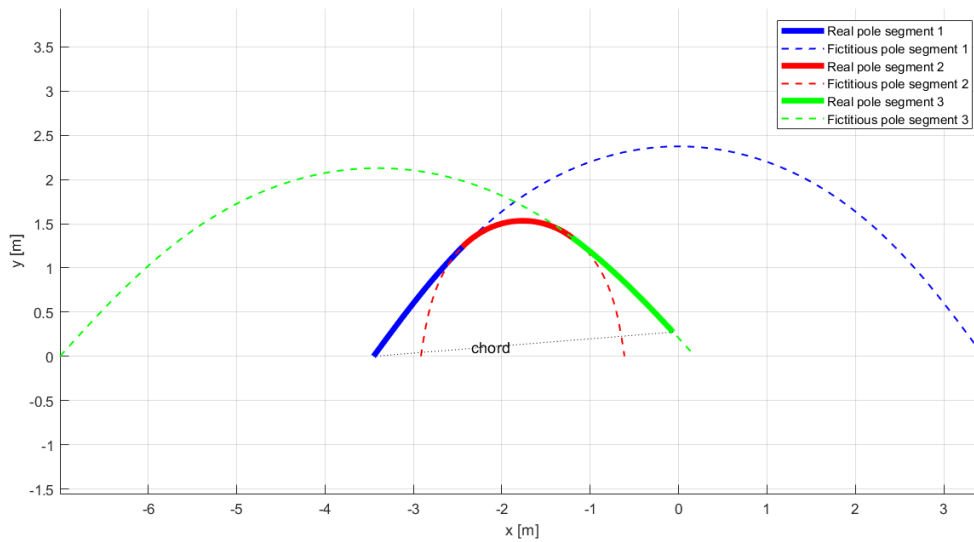


Figure D.2: Elastica solution for a pole having a high stiffness at its ends (Pole 2). The input properties are given in [Table D.1](#). The compressive end force R is found to be -1095 N.

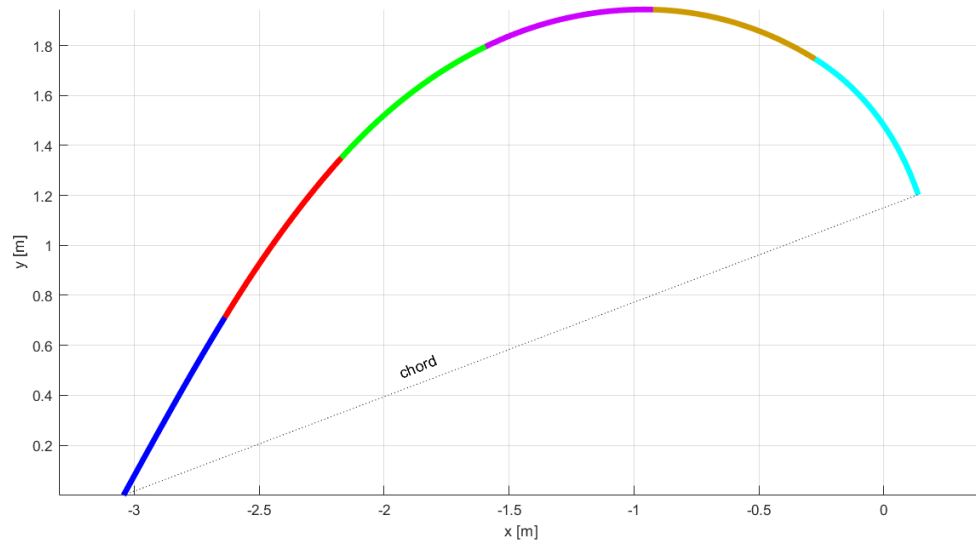


Figure D.3: Elastica solution for a variable stiffness pole. The pole properties are given in [Table D.2](#). The applied end torque T is $-1000 \text{ N} \cdot \text{m}$. The compressive end force R is found to be -832 N .

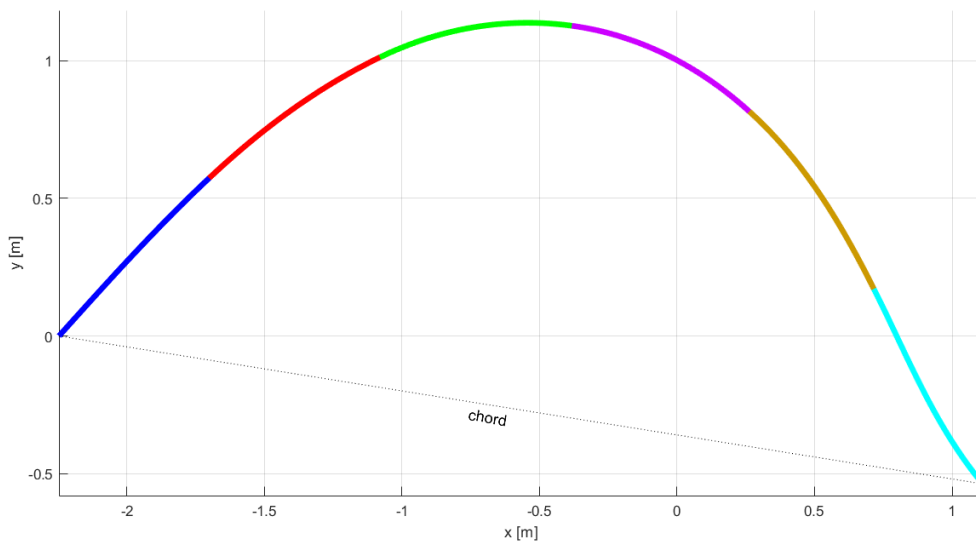


Figure D.4: Elastica solution for a variable stiffness pole. The pole properties are given in [Table D.2](#). The applied end torque T is $1000 \text{ N} \cdot \text{m}$. The compressive end force R is found to be -1861 N .

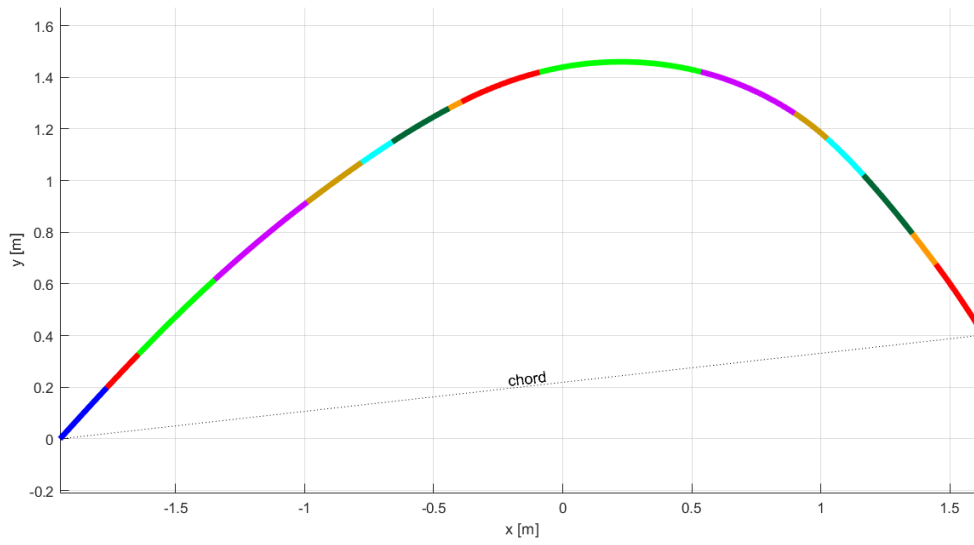


Figure D.5: Elastica solution for a variable stiffness pole consisting of 16 segments. The pole properties are given in [Table D.3](#). The compressive end force R is found to be -1242 N .

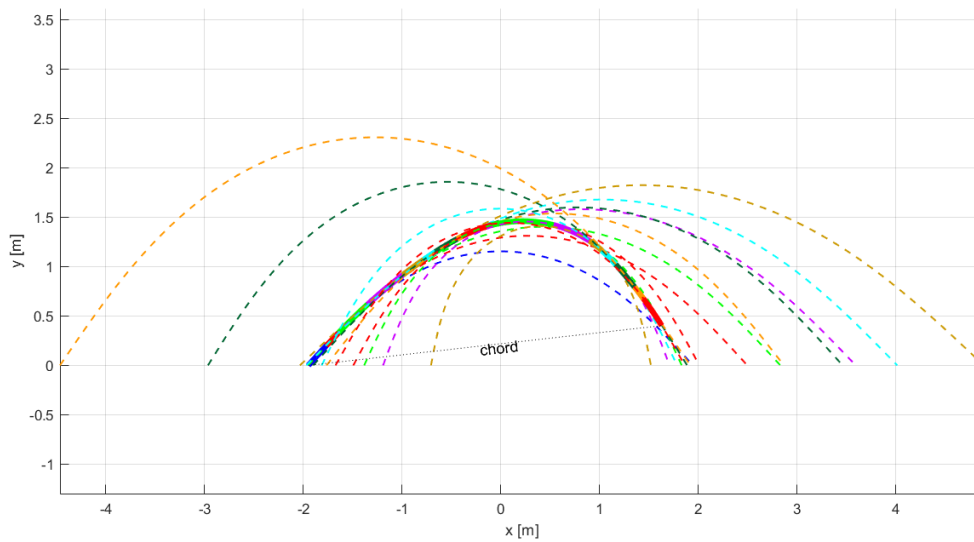
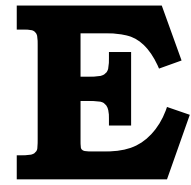


Figure D.6: Elastica solution for a variable stiffness pole consisting of 16 segments, including the fictitious poles. The pole properties are given in [Table D.3](#). The compressive end force R is found to be -1242 N .



Finding and updating the initial guess

At the start of the simulation, the solver needs an initial guess for the compressive force R and angle γ_1 to γ_n . The setting of these initial guess is described in [Appendix E.1](#). During the simulation, the initial guess has to be updated. The procedure for this is described in [Appendix E.2](#).

E.1. Setting the initial guess

For given input of segment lengths L_1 to L_n , pole chord l , applied end torque T and segments stiffnesses B_1 to B_n , the non-linear system solver 'fsolve' finds the values of the compressive force R and angles γ_1 to γ_n . In order to solve for these values iteratively, the solver needs an initial guess R_0 and γ_0 . γ_0 is an array of n elements, with n being the number of pole segments. The solver command in MATLAB looks as follows:

```
[OUT_ela, fval_ela, exitflag_ela] =  
    fsolve(@(x) variafunNb(x, INP_ela), X_ela, options) (E.1)
```

In [Eq. E.1](#) x is an array containing the values for R and γ . These values change during each iteration. X_ela consists of the initial guess R_0 and γ_0 . The solver input is saved in INP_ela . After solving, the solution for R and γ is given by OUT_ela . $fval_ela$ will give show how accurate the solution is.

$exitflag_ela$ will give a reason why the solver stopped. Preferably, the solver converges and $exitflag_ela$ will show that the non-linear system of equations is solved. If the solver does not converge to a solution, another initial guess should be chosen. The more segments a pole contains, the more sensitive the solver is to the initial guess which results in the solver diverging more often. A constant stiffness pole only needs one value for γ_0 and the solver will almost always converge. This fact is useful when determining a good initial guess for a pole consisting of multiple segments (and stiffnesses).

When finding a good initial guess for a variable stiffness pole, it is convenient to look at an equivalent constant stiffness pole. The solution for R and γ for this constant stiffness pole will be used as initial guess for the variable stiffness pole. To find the equivalent constant stiffness of the variable stiffness pole, the average stiffness of 4/5th of the pole is used, neglecting the first 1/5th of the pole. This first part of the pole is neglected as the stiffness is not influencing the deformation of the pole much, as this part of the pole is very close to the pole's x axis.

The average stiffness for the last 4/5th of the variable stiffness pole is calculated as follows. First,

L_{sum} is derived, containing the summations of the segment lengths.

$$L_{sum} = \left[\sum_{i=1}^1 L_i \quad \sum_{i=1}^2 L_i \quad \cdots \quad \sum_{i=1}^n L_i \right] \quad (E.2)$$

Note that the first term in L_{sum} is L_1 and the last term is the total pole length L_p . The average stiffness for the last 4/5th of the pole can now be calculated with:

$$B_{avg} = \frac{(L_{sum,j} - 1/5L_p)B_j + \sum_{i=j}^n (L_{sum,i} - L_{sum,i-1})B_i}{4/5L_p} \quad (E.3)$$

Here the index j is an integer between 1 and n and is chosen such that $L_{sum,j} > 1/5L_p$.

Next, using the inputs B_{avg} , L_p , T and l , the compressive force R_c and angle γ_c can be determined numerically¹. These values are used as initial guess for the variable stiffness pole as follows:

$$\begin{aligned} R_0 &= R_c \\ \gamma_0 &= [\gamma_c \ \gamma_c \ \cdots \ \gamma_c] \end{aligned}$$

E.2. Updating the initial guess

The values for R and γ , which are derived at the start of the vault, are used as initial guess for the next iteration. The compressive force R increases until MPB and decreases hereafter. This is shown in Fig. E.1.

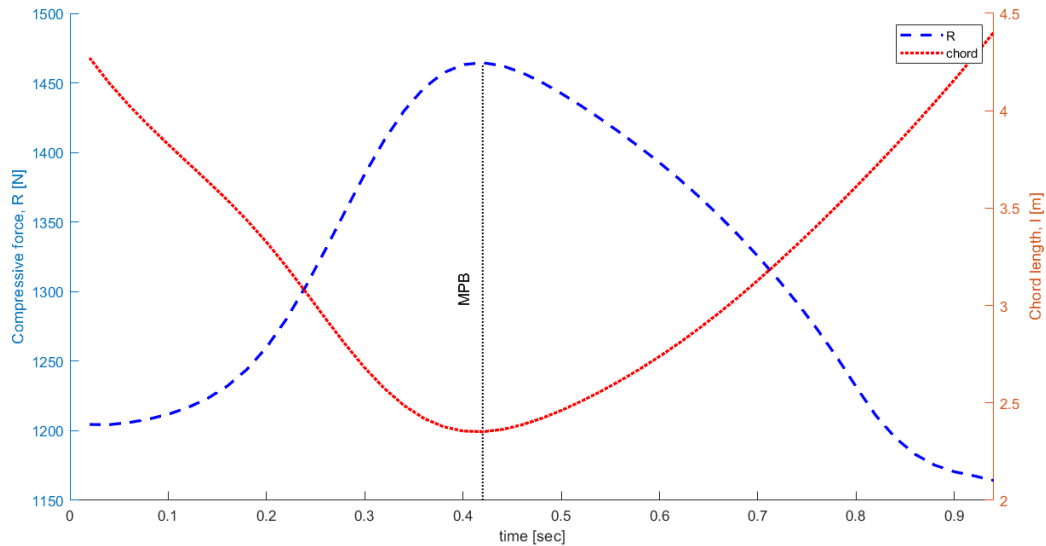


Figure E.1: Compressive force R and pole chord l during a vault. The MPB is indicated in the figure.

If the solver does not converge at any point, R_0 should be updated. Before MPB, a new R_0 is tried, which is larger than the previous guess. After MPB, a smaller R_0 is tried. If the solver keeps diverging, a new initial guess is derived, using the equivalent stiffness method explained in Appendix E.1.

¹Subscript c is used because these values apply to the equivalent constant stiffness pole

F

The non-linear system of equations

For an n -segment pole, $n+1$ unknowns need to be determined, while there are $3n$ boundary conditions. An approach of dealing with this overdetermined system will be presented in this Appendix. The equations in this Appendix are mostly extracted from the equations derived in [Appendix B](#).

Imagine a pole consisting of two segments, as shown in [Fig. F.1](#). The segments are part of two fictitious poles, which are also shown in the figure. The segment lengths and -stiffnesses are given by

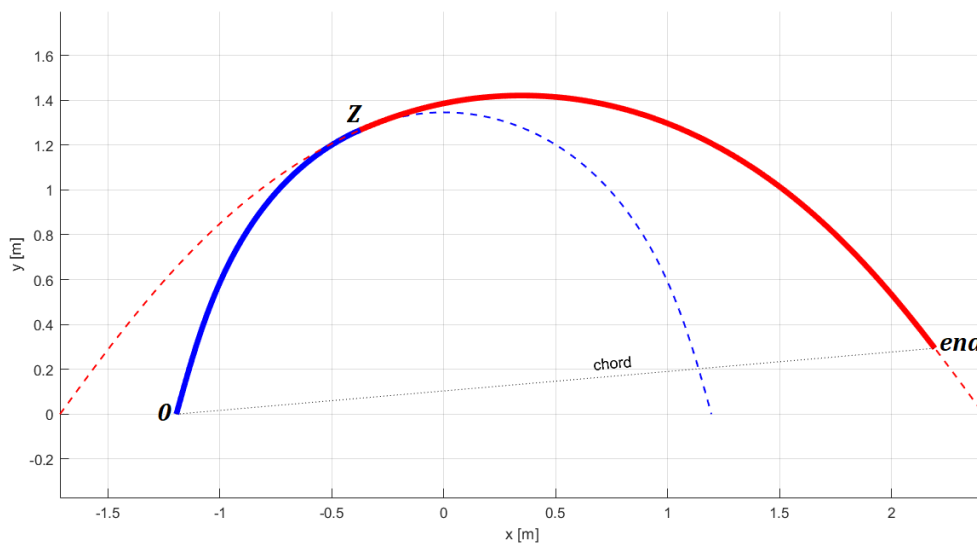


Figure F.1: A variable stiffness 2 segment pole

L_i and B_i , respectively. The pole chord l and end torque T are also known. The solver starts with an initial guess R_0 for R and γ_0 for γ . γ contains the angles for the tangent to the pole at $y = 0$ with the x axis of the two fictitious poles .

The moduli k_i are defined for each fictitious pole.

$$k_i = \sin \frac{1}{2} \gamma_i \tag{F.1}$$

The complete integral of the first kind is calculated using the built-in MATLAB function 'ellipke'.¹

$$K_i(k_i, \pi/2) = \text{ellipke}(k_i^2) \quad (\text{F.2})$$

The total length of the fictitious poles can now be calculated.

$$L_{fic,i} = \sqrt{\frac{B_i}{R}} 2K_i(k_i, \pi/2) \quad (\text{F.3})$$

The connection of the 2 segments in Fig. F.1 is named 'z'. Knowing the length of segment 1, the amplitude angle of the first segment at z is calculated with:

$$\phi_{1,z} = \pi \frac{L_1}{L_{fic,1}} - \frac{\pi}{2} \quad (\text{F.4})$$

Note that the first condition, the length of segment 1 being L_1 , is now met.

The position coordinates for the first fictitious pole at z can be calculated, using the curve shape equations derived in Appendix B.2.

$$x_{1,z} = \sqrt{\frac{B_1}{R}} (2E(k_1, \phi_{1,z}) - K(k_1, \phi_{1,z})) \quad (\text{F.5})$$

$$y_{1,z} = -\sqrt{\frac{B_1}{R}} 2k_1 \cos \phi_{1,z} \quad (\text{F.6})$$

The y coordinate at z is equal for both fictitious poles, so $y_{1,z} = y_{2,z}$.² Rewriting Eq. F.6, the amplitude angle of the second segment at z is given by:

$$\phi_{2,z} = -\arccos\left(-\frac{\sqrt{\frac{R}{B_2}} y_{2,z}}{2k_2}\right) \quad (\text{F.7})$$

If $y_{2,z}$ is larger than the top of the second fictitious pole, which lies at $\phi_{2,z} = 0$, $\phi_{2,z}$ is set to zero. The moment at z is given by:

$$M_{1,z} = R y_{1,z} \quad (\text{F.8})$$

$$M_{2,z} = -\sqrt{B_2 R} 2k_2 \cos \phi_{2,z} \quad (\text{F.9})$$

Note that $M_{1,z}$ is not necessarily equal to $M_{2,z}$, as $\phi_{2,z}$ could have been set to zero.

Next, a relation for the slope at z is established by combining Eq. B.9a and Eq. B.9b and re-arranging.

$$\theta_{1,z} = 2 \arcsin(k_1 \sin \phi_{1,z}) \quad (\text{F.10})$$

$$\theta_{2,z} = 2 \arcsin(k_2 \sin \pm \phi_{2,z}) \quad (\text{F.11})$$

Either $\pm \phi_{2,z}$ results in the same y_2 and $M_{2,z}$. The sign will be chosen such that the slopes $\theta_{1,z}$ and $\theta_{2,z}$ are closest (or equal). $\phi_{2,z}$ is updated if necessary.

Now the first equation is established, which incorporates the next two boundary conditions. The slopes of both fictitious poles should be equal at z, as well as the moments.

$$0 = (\theta_{1,z} - \theta_{2,z})^2 + (M_{1,z} - M_{2,z})^2 \quad (\text{F.12})$$

The two terms are squared to make sure that the slopes are equal and the moments are equal as well.³

¹Note that 'ellipke' uses k^2 as input argument instead of k .

²Note that the x coordinate at z is not equal for the fictitious poles, as the y_2 axis is shifted, w.r.t. the y_1 axis.

³Take e.g. $\theta_{1,z} - \theta_{2,z} = -5$ and $M_{1,z} - M_{2,z} = 5$. Subtracting these values will not equate to zero, so the terms should be squared.

The conditions at the pole end will be examined next. The x coordinate can be found in the same way as earlier.

$$x_{2,z} = \sqrt{\frac{B_2}{R}} (2E(k_2, \phi_{2,z}) - K(k_2, \phi_{2,z})) \quad (\text{F.13})$$

The second fictitious pole should be shifted horizontally, so that the poles are connected at z .

$$\Delta x_{12} = x_{1,z} - x_{2,z} \quad (\text{F.14})$$

The amplitude angle at the pole end is calculated as before. The fourth condition will then be met; the length of segment 2 is equal to L_2 .

$$\phi_{2,end} = \pi \frac{L_2}{L_{fic,2}} + \phi_{2,z} \quad (\text{F.15})$$

The coordinates at the pole end in the second fictitious pole coordinate system are given by:

$$x_{2,end} = \sqrt{\frac{B_2}{R}} (2E(k_2, \phi_{2,end}) - K(k_2, \phi_{2,end})) + \Delta x_{12} \quad (\text{F.16})$$

$$y_{2,end} = -\sqrt{\frac{B_2}{R}} 2k_2 \cos \phi_{2,end} \quad (\text{F.17})$$

The fifth boundary condition, the end torque T , is used to derive the next equation. The y location at the pole end is used.

$$\mathbf{0} = T - Ry_{2,end} \quad (\text{F.18})$$

Finally, the sixth boundary condition, the pole chord l , is applied to derive the final equation.

$$\mathbf{0} = l - \sqrt{(x_{2,end} - x_{1,0})^2 + y_{2,end}^2} \quad (\text{F.19})$$

The term $x_{1,0}$ is calculated with:

$$x_{1,0} = \sqrt{\frac{B_1}{R}} (2E(k_1, -\pi/2) - K(k_1, -\pi/2)) \quad (\text{F.20})$$

For a 2 segment pole, 3 unknowns have been determined, being R , γ_1 and γ_2 . In total 6 boundary conditions have been used to derive 3 equations. The system of non-linear equations is shown in Eq. F.21.

$$\underline{\mathbf{0}} = \begin{bmatrix} (\theta_{1,z} - \theta_{2,z})^2 + (M_{1,z} - M_{2,z})^2 \\ T - Ry_{2,end} \\ l - \sqrt{(x_{2,end} - x_{1,0})^2 + y_{2,end}^2} \end{bmatrix} \quad (\text{F.21})$$

The initial guess is updated iteratively until the vector of function values is near zero. The same approach can be used for a pole consisting of any number of segments.

G

Improving the production process

Current vaulting poles are produced by winding pre-impregnated fibers around a mandrel. This manufacturing process has been described in detail in [Section 2.3.5](#).

The design of the vaulting pole is limited because the mandrel has to be removed after curing of the resin. The pole diameter cannot be large in the middle and smaller at its ends. A tapered mandrel is often used as this allows for an easy removal. This results in the inner diameter being tapered as well. Also, a large prebend is prohibited, as this will also prevent (easy) removal of the mandrel.

Two alternative production processes are proposed. These processes do not impose the limitations described above on the design of the vaulting pole. The first method makes use of a female mould. The second method is similar to the current manufacturing method. Instead of metal mandrel a dis-solvable mandrel is used.

G.1. Female mould

In the first alternative production process a female mould is used. The shape of the pole is milled out of two large metal blocks. Pre-impregnated fiber cloth is placed inside the hollow out metal block. The materials is placed such that the desired lay-up is obtained. Then a silicone tube is placed on top. The fibers are wrapped around the tube properly and the second metal block is placed on top. Next the tube is pressurized by air, so that the pole material is pressed against the two metal blocks tightly. An overview of this set-up is shown in [Fig. G.1](#). The pre-preg material is now cured in an oven.

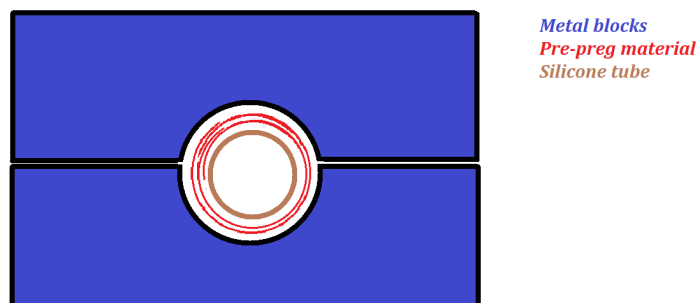


Figure G.1: Cross-sectional overview of the production process, using a female mould

The advantages of this production process is that the design of the pole is not limited in any way.

The pole is allowed to have a large prebend. Also the inner diameter can be distributed over the length of the pole as desired. The draw-backs are:

- The fibers are not continuous.
- The mould is very expensive,
- The pole is limited to the shape of the mould.

G.2. Soluble or meltable mandrel

Another way of producing the pole could be by using a dissolvable or meltable mandrel, instead of a metal mandrel. The same filament winding process can be used, as currently applied. After the curing process, the mold is removed by solving it in warm water or by applying heat and melting it.

The big advantage is again that the pole is not limited in any way. The disadvantages of this production method are:

- The mold cannot be re-used again.
- Curing in a hot oven or autoclave does not work. The mold material will sag around 60°C in case of a soluble mandrel (Benchhoff, 2017). In case of a meltable mandrel, the melting point is usually ranged between 20°C and 200°C (Lemer, 2018).
- The mold material might break during the filament winding process, as the material is not as strong as a metal mold. This can be prevented by using pole free filament winding (Kattukaren, 2010).

Bibliography

- J. Frère, M. L'Hermette, J. Slawinski, and C. Tourny-Chollet, *Mechanics of pole vaulting: a review*, *Sports Biomechanics* **9**, 123 (2010), PMID: 20806847.
- S. Burgess, *The modern olympic vaulting pole*, *Materials & Design* **19**, 197 (1998).
- J. Morlier and M. Mesnard, *Influence of the moment exerted by the athlete on the pole in pole-vaulting performance*, *Journal of biomechanics* **40**, 2261 (2007).
- M. F. Ashby and D. Cebon, *Materials selection in mechanical design*, *Le Journal de Physique IV* **3**, C7 (1993).
- N. P. Linthorne, *Energy loss in the pole vault take-off and the advantage of the flexible pole*, *Sports Engineering* **3**, 205 (2000).
- IGS, *How gas springs work* (2017), [Online; accessed 19-November-2017].
- M. Reijne, *The next level in pole vaulting*, (2016).
- T. Fukushima, S. Nishikawa, K. Tanaka, and Y. Kuniyoshi, *Transitional buckling model for active bending effect in pole vault*, in *6th International Symposium on Adaptive Motion of Animals and Machines (AMAM)* (2013).
- N. Linthorne, *Design and materials in athletics*, Vol. 2 (Elsevier, 2007) p. 296.
- D. Nielson, *Athletics outstanding performer - the vaulting pole*, (2006).
- M. Hubbard, *Dynamics of the pole vault*, *Journal of Biomechanics* **13**, 965 (1980a).
- G. Griner, *A parametric solution to the elastic pole-vaulting pole problem*, *Journal of Applied Mechanics* **51**, 409 (1984).
- A. Arampatzis, F. Schade, and G.-P. Brüggemann, *Effect of the pole-human body interaction on pole vaulting performance*, *Journal of biomechanics* **37**, 1353 (2004).
- F. Schade, J. Isolehto, A. Arampatzis, G. Brüggemann, and P. Komi, *Biomechanical analysis of the pole vault at the 2005 iaaf world championships in athletics extracts from the final report*, *New Studies in Athletics* **22**, 29 (2007).
- J. Morlier and M. Cid, *Three-dimensional analysis of the angular momentum of a pole-vaulter*, *Journal of biomechanics* **29**, 1085 (1996).
- F. Schade, A. Arampatzis, and G.-P. Brüggemann, *Reproducibility of energy parameters in the pole vault*, *Journal of biomechanics* **39**, 1464 (2006).
- R. Boiten, *Nominated lecture: The mechanics of instrumentation*, *Proceedings of the Institution of Mechanical Engineers* **177**, 269 (1963).
- C. L. Davis and S. N. Kukureka, *Effect of materials and manufacturing on the bending stiffness of vaulting poles*, *Physics Education* **47**, 524 (2012).
- M. Strangwood and A. Subic, *Modelling of materials for sports equipment*, *Materials in Sports Equipment* **2**, 3 (2007).
- G. Liu, S.-K. Nguang, and Y. Zhang, *Pole vault performance for anthropometric variability via a dynamical optimal control model*, *Journal of Biomechanics* **44**, 436 (2011).

- N. Linthorne, *Mathematical model of the takeoff phase in the pole vault*, Journal of Applied Biomechanics **10**, 323 (1994).
- W. Johnson, S. Al-Hassani, and R. Lloyd, *Aspects of pole vaulting mechanics*, Proceedings of the Institution of Mechanical Engineers **189**, 507 (1975).
- F. Schade and A. Arampatzis, *Influence of pole plant time on the performance of a special jump and plant exercise in the pole vault*, Journal of biomechanics **45**, 1625 (2012).
- H. Gros and V. Kunkel, *Biomechanical analysis of the pole vault*, Scientific research project at the games of the XXIVth olympiad-Seoul 1988 , 219 (1990).
- R. M. Angulo-Kinzler, S. B. Kinzler, X. Balias, C. Turro, J. M. Caubet, J. Escoda, and J. A. Prat, *Biomechanical analysis of the pole vault event*, Journal of Applied Biomechanics **10**, 147 (1994).
- N. Linthorne, *4 energy transformations in the pole vault*, Physics of sports (2012).
- M. Hubbard, *An iterative numerical solution for the elastica with causally mixed inputs*, Transactions of the ASME **47**, 200 (1980b).
- H. Walker and P. Kirmser, *Computer modeling of pole vaulting*, Mechanics and sport **4**, 131 (1973).
- R. Q. van der Linde and A. L. Schwab, *Multibody dynamics b*, (2011).
- R. V. Southwell *et al.*, *Introduction to the theory of elasticity for engineers and physicists*, (1941).
- A. E. H. Love, *A mathematical treatise on the theory of elasticity*, Dover Books (1944).
- H. Adamczewski and B. Perlt, *Run-up velocities of female and male pole vaulting and some technical aspects of women's pole vault*, New studies in athletics **12**, 63 (1997).
- P. McGinnis and L. Bergman, *A dynamic finite element model of pole vaulting*, Journal of Biomechanics **16**, 287 (1983).
- J. Morlier, M. Mesnard, and M. Cid, *Pole-vaulting: identification of the pole local bending rigidities by an updating technique*, Journal of applied biomechanics **24**, 140 (2008).
- M. Ekevad and B. Lundberg, *Simulation of 'smart'pole vaulting*, Journal of Biomechanics **28**, 1079 (1995).
- M. van den Bosch, *Explore pole vaulting strategies by control optimization*, (2018).
- B. Benchoff, *Soluble molds for composite parts*, (2017).
- Lemer, *Melttable core*, (2018).
- K. Kattukaren, *The design, prototyping and testing of a pole free filament winder*, (2010).